ACCELERATION-DISPLACEMENT RESPONSE SPECTRA (ADRS) FOR
DESIGN OF SEISMIC ISOLATION SYSTEMS IN TURKEY

by

Aslıhan Yolcu

B.S, Civil Engineering, Kocaeli University, 2012

Submitted to Kandilli Observatory and Earthquake Research Institute
in partial fulfillment of the requirements for the degree of
Master of Science

Graduate Program in Earthquake Engineering

Boğaziçi University

2018

ACCELERATION-DISPLACEMENT RESPONSE SPECTRA (ADRS) FOR DESIGN OF SEISMIC ISOLATION SYSTEMS IN TURKEY

APPROVED BY:

Assoc. Prof. Dr. Gülüm Tanırcan   . . . .
(Thesis Supervisor)

Cüneyt Tüzün, Ph.D   . . . .
(Thesis Co-supervisor)

Prof. Dr. Erdal Şafak   . . . .

Assoc. Prof. Dr. Eren Uçkan   . . . .

Assist. Prof. Dr. Ahmet Anıl Dindar   . . . .

DATE OF APPROVAL: 10.01.2018

ACKNOWLEDGEMENTS

ABSTRACT

ACCELERATION-DISPLACEMENT RESPONSE SPECTRA (ADRS) FOR DESIGN OF SEISMIC ISOLATION SYSTEMS IN TURKEY

Nonlinear Response History Analyses (NLRHA) have been frequently used in seismic isolation system design since the displacement at long period end of the code-based spectra is limited to a certain value and may not accommodate larger displacement demands. The NLRHA is a practical tool to determine the maximum displacement of the system based on predefined values of effective period, effective damping and base shear transmitted to superstructure which are internally connected and requires an iterative process. In order to reduce the process, the methodology which is called as Acceleration-displacement response spectra (ADRS) approach is proposed by Whittaker and Jones (2013, 2014).

In this study, ADRS approach is extended considering the new Turkish Building Seismic Design Code (TBSDC, 2018) that will come into force in 2018. Series of nonlinear response history analyses are performed for several isolation system parameters and seismic hazard levels. Displacement spectra are obtained by using bi-linear hysteresis curve model. Effective and robust ADRS graphs which facilitate the preliminary design stage of the seismic isolation systems are obtained in terms of acceleration and displacement demands of earthquakes. The effects of differences in fundamental seismic isolation system parameters and ground motion selection criteria on the preliminary design of seismic isolation systems are examined and represented in graphical forms.

ADRS graphs provide the base shear and displacement limits of seismic isolation systems in the region under maximum considered earthquake (DD1) and design basis earthquake (DD2) design levels. Shaking levels are obtained from New Probabilistic

Seismic Hazard Map of Turkey (TDTH, 2016). The design spectra composition is formed using two site categories (NEHRP C and NEHRP D) and two hazard zones (high and moderate hazard) at each design level. For each design spectra, eleven horizontal ground motion pairs are selected and linearly scaled using the geomean spectral ordinates. Analyses are performed using a combination of eight site-specific design spectra in total, six effective isolation system periods and five yield levels.

Evaluation and discussion of the ADRS graphs are provided to develop an overall understanding about the base shear and displacement limits of a seismic isolation systems in the region.

ÖZET

TÜRKİYE'DE SİSMİK YALITIM SİSTEMLERİNİN TASARIMINDA İVME-YERDEĞİŞTİRME TEPKİ SPEKTRUMLARI

Yönetmeliklerde yer alan spektrumların uzun periyodundaki yer değiştirme belirli bir değer ile sınırlandırılmıştır ve daha büyük yer değiştirme taleplerini karşılamayabilir bu nedenle doğrusal olmayan tepki spektrumu analizleri (NLRHA), sismik izolasyon sistem tasarımında sıklıkla kullanılmaktadır. NLRHA, önceden tanımlanmış etkin periyot, etkin sönüm ve üst yapıya aktarılan kesme kuvveti gibi birbirine bağımlı ve tekrarlama yöntemi gerektiren parametrelere dayanan sistem maksimum yer değiştirmesini belirlemek için pratik bir araçtır. Tekrarlama sürecini azaltmak için, Whittaker ve Jones (2013, 2014) tarafından ivme-yer değiştirme tepki spektrumu yöntemi önerilmiştir.

Bu çalışmada, 2018 yılında yürürlüğe girecek yeni Türkiye Bina Deprem Yönetmeliği (TBDY, 2018) dikkate alınarak ADRS yaklaşımı genişletilmiştir. Çeşitli yalıtım sistemi parametreleri ve sismik tehlike seviyeleri için bir takım doğrusal olmayan tepki analizleri gerçekleştirilmiştir. Yer değiştirme spektrumu, bi-lineer çevrim eğrisi modeli kullanılarak elde edilmiştir. Sismik izolasyon sistemlerinin ön tasarım aşamasını kolaylaştıran etkili ve sağlam ADRS grafikleri, deprem ivme ve yer değiştirme talepleri cinsinden elde edilmektedir. Temel sismik izolasyon sistemi parametreler ve yer hareketi seçim kriterlerindeki farklılıkların sismik izolasyon sistemlerinin ön tasarımı üzerindeki etkileri incelenmiş ve bulgular grafiksel biçimlerde sunulmuştur.

ADRS grafikleri, bölgedeki sismik yalıtım sistemi taban kesme kuvveti ve yer değiştirme limitlerini en büyük deprem yer hareketi düzeyi (DD1) ve standart tasarım deprem yer hareketi düzeyi (DD2) tasarım seviyeleri için elde edilmesini sağlamaktadır. Sarsma seviyeleri Türkiye Yeni Olasılıksal Sismik Tehlike Haritası'ndan alınmıştır (TDTH,

2016). Tasarım spektrumları, her bir tasarım seviyesinde, iki zemin sınıfı (NEHRP C ve NEHRP D) ve iki tehlike bölgesi (yüksek ve orta tehlike) kullanılarak oluşturulmuştur. Her bir tasarım spektrumu için, onbir yatay yer hareket çifti seçilmiştir ve geomean spektral ordinatları kullanılarak doğrusal ölçeklendirme yapılmıştır. Analizler toplamda sekiz adet bölgeye özgü tasarım spektrumu, altı etkin sismik yalıtım sistemi periyodu ve beş akma seviyesi kombinasyonu kullanılarak yapılmıştır.

Bölgedeki kesme kuvveti ve yerdeğiştirme sınırlarına dair etraflı bir kavrama geliştiştirmek amacıyla ADRS grafiklerinin değerlendirilmesi ve tartışılmasına yer verilmiştir.

TABLE OF CONTENTS

LIST OF FIGURES

LIST OF TABLES

LIST OF SYMBOLS

D	Average displacement
f_b	Force in the isolator
F_S	Site coefficient for short period
F_1	Site coefficient for 1 s period
g	Acceleration of gravity
k_1	Elastic stiffness
k_2	Post-elastic stiffness
m_t	The total mass above the isolation device
M_w	Moment magnitude
Q_d	Strength on yield force
R	Earthquake force reduction factor
R_c	Radius of shear surface curvature of a seismic isolation unit
R_{jb}	Joyner and Boore distance
S_a	Spectral acceleration
S_{ae}^{DD1}	Lateral spectral acceleration for %5 damping at maximum ground motion level (g)
S_{DS}	Short period design spectral acceleration coefficient
S_{D1}	Design spectral acceleration coefficient for 1 s period
S_1	Hazard map spectral acceleration coefficient for 1 second period
SR	Strength ratio *or* yield ratio
S_S	Hazard map spectral acceleration coefficient at short period
S_1	Spectral acceleration coefficient for 1 s period
T	Period
T_M	The effective vibration period of seismically isolated building at maximum displacement
T_1	The first slope of period of vibration
T_2	The second slope of period of vibration
u_i	Deformation of seismic isolation system

$\ddot{u}_g(t)$	Ground acceleration
v_i	Velocity of seismic isolation system
V_M	Base shear which is transmitted to superstructure
$(V_s)_{30}$	The average shear wave velocity between 0 and 30 metres depth (m/s)
W	System weight
W_d	Dissipated energy, the area inside the force-displacement curve
z	Fraction of the yield strength
α	post-to-pre yield stiffness ratio
γ_F	Fault distance coefficient
Δ	Displacement
Δ_y	Yield deformation
η	Damping scaling coefficient
μ	Effective friction coefficient
ξ	Damping ratio
ω	Circular frequency

LIST OF ACRONYMS/ABBREVIATIONS

ADRS	Acceleration-Displacement Response Spectra
DD1	Maximum Considered Earthquake, MCE
DD2	Design Basis Earthquake, DBE
FN	Fault normal
FP	Fault parallel
FPS	Friction pendulum system
GM	Geometric mean (or) geomean
HDBR	High-damping natural rubber bearings
HH	High hazard
LRB	Lead-rubber bearings
MH	Moderate hazard
SDOF	Single degree of freedom
SRSS	Square root of the sum of the squares
NLRHA	Nonlinear response history analysis
TBSDC	Turkish Building Seismic Design Code
TDTH	New Probabilistic Seismic Hazard Map of Turkey
PEER	Pacific Earthquake Engineering Research

1. INTRODUCTION

1.1. Objectives of the Study

Damped elastic spectra (5%) which are produced for fixed-base structures are not sufficient to evaluate highly damped seismically isolated buildings. Although seismic isolation devices represent hysteresis behaviour in real life, engineers generally use equivalent viscous damping assumption or some scale factors which are defined in international codes to represent the highly damped behaviour of the seismic isolation units. The equivalent viscous damping methodology requires use of internally connected parameters and it makes the calculations iterative and indirect. Hence the objective of this study is to perform practical and direct Acceleration-displacement response spectra (ADRS) methodology to obtain standardized graphics which make the preliminary design of seismic isolation systems easier.

ADRS graphs which are obtained in the study reduce the iterative procedure and aims to fulfill the needs of both practical engineering and technological development needs in design of seismic isolation systems.

1.2. Justification for the Study

The hazardous effects of earthquakes cause collapse of many conventionally-built existing structures and damage of new buildings in Turkey. The life safety performance level was an acceptable criterion which lets the damage of the structure without any life-loss of the people. Although preventing human life-loss still plays an important role in design process, it is not the only concern of the owners and designers anymore. In recent years, comfort limits, life-cycle cost of the structure, and economic write-offs have been also dominated the design process. Investors do not only want from designers to prevent damage of structural and non-structural members but also, they want to protect and maintain the functionality of valuable equipment and instruments which are inside the building. Even if a destructive earthquake occurs in expected life-

time of structure, several buildings such as hospitals, database centers, buildings which contain energy systems, commercial buildings which have contribution to economy of the countries should continue to serve without any damage.

Usage of seismic isolation systems is the most effective and rational alternative solution to minimize damage and to reach the required performances because they enable to dissipate energy. Also, seismic isolation units can be used in retrofitting projects of important buildings without any intervention on superstructure.

Principles of Nonlinear Response History Analysis (NLRHA) techniques have been permanently updated in seismic codes and besides the use of seismically isolated systems which requires detailed evaluation of ground motions has been significantly increased. Nonlinear Response History Analyses have been frequently used in the design of earthquake isolation systems since the displacement at long period end of the code based spectra is limited to a certain value and may not accommodate larger displacement demands.

The NLRHA serves a practical tool to determine the maximum displacement of the isolation system based on predefined values of effective period, effective damping and base shear transmitted to superstructure. Since the above mentioned isolation system parameters are internally connected to each other iterative process is required. In order to reduce the process, the methodology which is called ADRS involves a series of nonlinear response history analyses introduced. When the increasing implementation of seismic isolation system is considered, time saving and handy methodology which can be used for both lead rubber bearings and friction pendulum bearings is needed. The proposed methodology can be repeated for different isolation periods and yield levels for different seismic input levels to obtain a family of ADRS graphs. These graphs serve an effective and robust tool for the preliminary design stage of seismic isolation systems.

In addition to that, the methodology makes it possible to calculate the base shear, displacement of seismic isolation system and effective period rapidly in the preliminary

design stage. Hence, designers may evaluate/compare the pre-defined values suggested by the manufacturers and those provided with ADRS.

1.3. Outline

In Chapter 2, a literature review of the study is provided. The literature review is separated into three subtitles. General definitions and properties of seismic isolation systems are described. The essential conditions for seismic isolation systems, applications of the method worldwide, types of the isolation devices are indicated. The nonlinear procedure and the ADRS methodology are explained.

Chapter 3 presents the description of the ADRS methodology, base isolation system parameters and application of equation of motion for a single degree of freedom (SDOF) oscillator which represents the bi-linear seismic isolation system model.

In Chapter 4, the flow chart of analyses is given. The identification of ground motion input data which is used in nonlinear analysis is made. Ground motion selection criteria and scaling procedures are described. Afterwards, the ground motions which were used in current analyses are demonstrated. The design hazard levels and nonlinear analysis procedure are presented in the same chapter.

In Chapter 5, the analyses results which are represented as ADRS graphs for certain periods and yield levels are exhibited. Also, comments on results and comparison of graphs with each other are given here.

Lastly, Chapter 6 presents the conclusions of study.

2.   LITERATURE REVIEW

2.1. General Definition and Properties of Seismic Isolation Systems

Tüzün and Şadan (2017) indicated that, when the historical background is studied, the first examples of seismic isolation systems in the history are seen during Persian Empire period. People placed stone blocks without mortar between foundation and grave to let them move during the earthquake (B.C. 530). Then, they constructed structures which can make rocking movement. The Obelisk which exists in Sultanahmet can be given as an example of this type of structure. The work is placed on four bronze cubes which are located in each corner of base. (A.D. 379-395) The use of modern seismic isolation started in New Zealand in 1970. The first seismic isolation system application was made in the USA, in 1985.

Seismic isolators are flexible in horizontal direction and rigid in vertical direction. Their horizontal rigidity is respectively smaller than the superstructure. Consequently, it can be assumed that superstructure makes a rigid body motion upon the seismic isolation unit. Seismic isolation system design aims to increase the period of the structure by reducing stiffness of structure. Also, it increases the damping and energy dissipation capability of structure. Fixed-base structures reach 5% damping ratio, but seismically isolated structures may have 15% or even more damping ratio.

Naeim and Kelly (1999) explained the basic definitions, the use of seismic isolation among the other countries and design methodologies. They explained all types of seismic isolation bearings. In this study, only the names of the various seismic isolation bearings are presented and two widely used types of seismic isolation systems are explained.

Seismic isolation systems can be separated into two groups: (1) elastomeric (rubber) based systems and (2) isolation systems based on sliding. Elastomeric bearings can be subdivided as low-damping natural or synthetic rubber bearings, high-damping

natural rubber bearings (HDNR), lead-rubber bearings (LRB). Sliding bearing have following subgroups; pure friction system, friction pendulum system (FPS), sliding isolation pendulum bearings, resilient friction base system. Schematic representations of elastomeric and sliding bearings are indicated below in Figure 2.1 and 2.2.
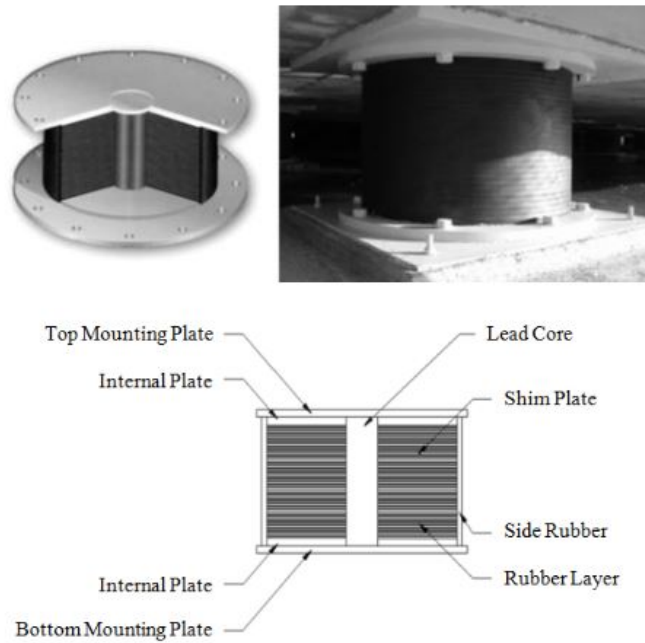
Figure 2.1. Elastomeric bearing.
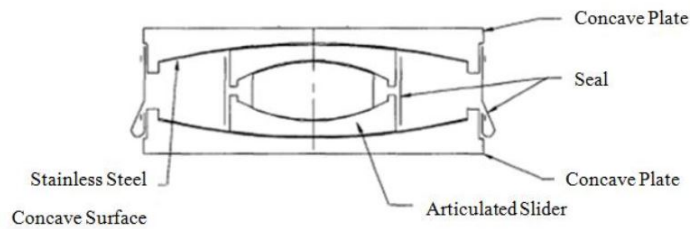
Figure 2.2. Sliding bearing.

In recent years, lead rubber and friction pendulum bearing types of seismic isolators which represent hysteretic behavior have been generally used by the designers. Seismic isolation design is based on reducing seismic response of the structure by providing natural vibration period and displacement capability increment of the struc-

ture. Seismic isolators have flexibility in horizontal direction since they dissipate large amounts of energy during the earthquake and mitigate the shaking compared to fixed base buildings. In lead rubber bearing, lead core provides damping and steel layers provide vertical rigidity. When there is a need for small horizontal rigidity, friction pendulum bearings meet the needs. If structures with friction pendulum bearings are not exposed to a lateral force which overcomes the friction force, the system works as a fixed-base system. For that reason, in small earthquakes, system with friction pendulum bearings may not be activated. Besides, this property can be an advantage for structures which exists in windy region.

Although seismic isolation units are generally implemented in bridges, only a few buildings facilitate with base isolation from all around the world. There are various reasons of it and the most common reason not to apply base isolation to buildings is the cost arose when the construction is first manufactured.

Chatzidaki (2011) examined the life-cycle cost of the structure with a base isolation. Different analysis procedures are shown such as linear static procedure, nonlinear static procedure and nonlinear dynamic procedure which can be subdivided incremental dynamic analysis, multi-component incremental dynamic analysis, and multiple-stripe dynamic analysis. Then, the optimum design of base isolated reinforced concrete structures is represented in terms of life-cycle cost analysis. The life-cycle cost of conventional building, seismically isolated with lead rubber bearing and seismically isolated with high damping natural bearing are compared and results are shown in graphical form. As a result, in all cases, seismically isolated structures are cost less than conventional building in long term because they make it possible to protect both structural and non-structural members of the building and necessitate less retrofitting than fixed-base building.

2.2. Nonlinear Analysis Procedure

2.2.1. Nonlinear Response History Analysis (NLRHA)

Engineering design parameters such as displacement and base shear dominate the seismically isolated structure design. Seismic isolation systems are highly damped systems and they show hysteresis behavior. Engineers generally define the hysteresis behavior of seismic isolation systems in accordance with equivalent linear system with secant stiffness or equivalent viscous damping approach which has been proposed by several design codes from all around the world. Jones *et al.* (2015) explained that, seismic isolation systems cannot be considered as linear systems and described accurately by the linear approaches. Also, the design necessitates displacement based design instead of force based design procedure to satisfy the target performance levels. At this stage, NLRHA is adopted for performance-based earthquake engineering to understand the nonlinear mechanism of the seismic isolation systems. NLRHA provides the observation of critical forces on the structural members and helps to evaluate these forces to let the system remain elastic. On the other hand, equivalent viscous damping approach is response dependent and requires an iterative process. For that reason, having a robust and immediate tool on the preliminary design stage is needed for designers to have a quick point of view about inelastic seismic demands of seismically isolated systems.

Bülbül (2011) described that the strength based design has some limitations and shortcomings compared to performance based design. Inelastic deformation demands of structural members may not be predicted very well. In the inelastic behavior stage, several structural members may yield and force and story drift distribution may change. It should be taken into consideration for realistic design because distribution change can not be predicted by strength reduction factor and linear elastic analysis procedures accurately. Strength reduction factors which are defined in seismic design codes may not be sufficient to estimate the strength and ductility capacity of existing building. Elastic analysis may not be sufficient to catch the great deformation demands in critical locations which may induce a story mechanism in the first or upper floors of the

building.

The hysteresis behavior of the seismic isolation system is indicated by using bi-linear hysteresis curve model for the study because it is a simple way of describing nonlinear behavior of the system. In PRISM for Earthquake Engineering software (PRISM, 2018) which is used in the analyses; there are other alternative models of hysteresis curve description, such as tri-linear, Bouc-wen, modified- tekada, al-bermani.

Chatzi (2017) demonstrated the modeling of hysteresis, by describing the details of Bouc-wen model and introducing other models which are used to meet different needs of designers, such as Clough bi-linear stiffness degrading model which represents bending, bi-linear origin-oriented model which represents shear. Also, there are modified Ibarra-Medina-Krawinkler deterioration model which is calibrated on steel beam to column connections and Stewart degrading stiffness.

2.2.2. Acceleration-Displacement Response Spectra

The ADRS approach has been suggested by Whittaker and Jones (2013, 2014) to represent realistic behavior of seismic isolation systems, to diminish analyses time by elimination of iterative process and produce an accurate tool. The ways of transformation from seismic design spectra which are defined for fixed-base buildings in building codes to seismic design spectra for seismically isolated buildings are examined. They used "B factors" which is defined in different international codes to transform elastic code spectra (5% damped) to highly damped spectra and equivalent viscous damping approach to obtain design spectra for isolated structures. They compared elastic acceleration and displacement responses of 25% equivalent response damping which represents isolated building to 5% damped code defined spectra of the 2011-Christchurch earthquake. Results showed that, if there was an option to build seismically isolated buildings before the Christchurch earthquake, structures would not be affected from damages of the earthquake as conventional buildings.

Afterwards, Jones *et al.* (2015) performed case studies including near field sites

in various seismically active regions such as New Zealand, Wellington. Analyses are made for two hazard levels (1000 years, 2500 years). Seven pairs of records are used to obtain the ADRS charts. In case of Wellington site specific study, firstly, they took principal components of the records to produce ADRS graphs. Secondly, they combined maximum responses of two direction using SRSS. Then, they took the average of seven SRSS results to produce ADRS graphs. They have observed that there is not notable difference between those two cases. In San Francisco region they scaled records in time-domain and frequency domain and showed that there are consistent results with each other. In long period range of the ADRS graphs the displacement responses are higher as it expected for a near fault region. In the same year, they performed other case studies in Turkey, New Zealand and California. They shared site-specific investigations and discussed whether or not equivalent viscous damping approach is amenable to ADRS in lack of NLRHA.

Jones *et al.* (2017) explored the effect of scaling condition on the ADRS graphs. ADRS results are indicated for unscaled records, linearly scaled records in time domain and records scaled in frequency domain. They have utilised the Maule (Mw = 8.8), Iquique (Mw = 8.2) and Illapel (Mw = 8.3) earthquakes as cases studies. As a result, linearly scaled results give greater base shears and displacements compared to frequency-domain scaling. Isolation base shear and displacements are consistent with the common Chilean design values for frequency-domain scaled set of records. The most significant motions in the study are the motions which are recorded at Concepcion Centro station during Maule earthquake. The contribution of the records of Conception City which are overlain by deep soft soil deposits cause large displacement and base shears at 2.0 seconds period of both for Maule records ADRS graphs and all records ADRS graphs.

3. DESCRIPTION OF THE METHODOLOGY

3.1. System Parameters

In the current study, seismic isolation system considered as a single degree of freedom (SDOF) oscillator which represents hysteresis behavior. Although, there are several types of hysteresis curves, bi-linear hysteresis curve models have been used to represent nonlinear behavior of a typical seismic isolation system which is represented schematically in Figure 3.1.
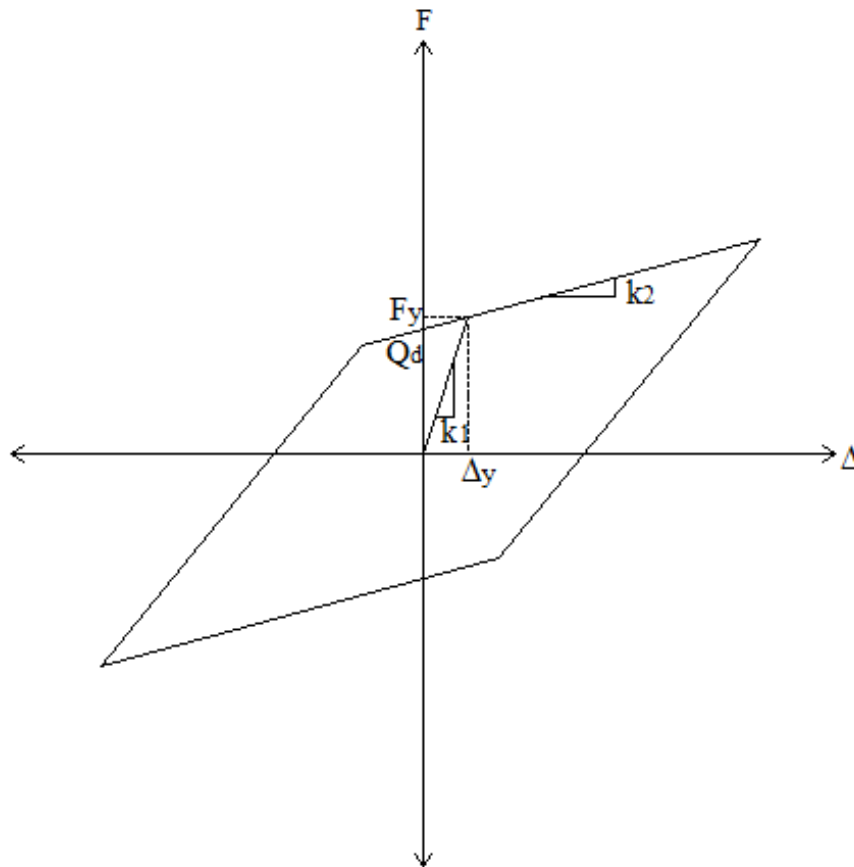
Figure 3.1. Bi-linear curve representation.

Based on the information from the manufacturers and practicing engineers, it is assumed that the elastic stiffness (k_1) is 10 times greater than characteristic stiffness

(k_2) in analyses hence the properties of seismic isolation are dominated by the assigned post-yield stiffness (k_2) and yield level (Q_d). Yield level can also be called as "strength ratio on yield force" and it expresses "characteristic strength" of a seismic isolator. When the typical two seismic isolator types are evaluated; (k_2) is stiffness of rubber, (Q_d) is the lead core yield force for lead rubber bearings and friction force for friction pendulum bearings. (k_2), expresses the "characteristic stiffness" of a seismic isolator namely, the second slope of force-displacement graph of bi-linear curve. As such, the seismic isolation system can be defined in terms of yield level and post-yield stiffness period of vibration.

As shown below, the post-to-pre yield stiffness ratio (α), the second slope period of vibration (T_2) and strength ratio (SR) are calculated by the Equations 3.1, 3.2 and 3.3.

$$\alpha = \frac{k_2}{k_1} \tag{3.1}$$

$$T_1 = T_2\sqrt{\alpha} \tag{3.2}$$

$$SR = \frac{Q_d}{W} \tag{3.3}$$

where, W is the system weight and T_1 is the first slope period of vibration.

3.2. Equation of Motion

Isolation system response which gives shape to ADRS lines is determined by time history analyses of a bi-linear hysteresis SDOF oscillator. Namely, the system can be idealized as a rigid mass mounted on a single isolator as it is explained in the paper of Chopra *et al.* (2004) to represent the nonlinear behavior of the isolation systems.

The nonlinear equation of motion described for the SDOF system is calculated

as defined below:

structure

isolation
device

m_t

u_i

k_2
Q_d

$\ddot{u}_g(t)$
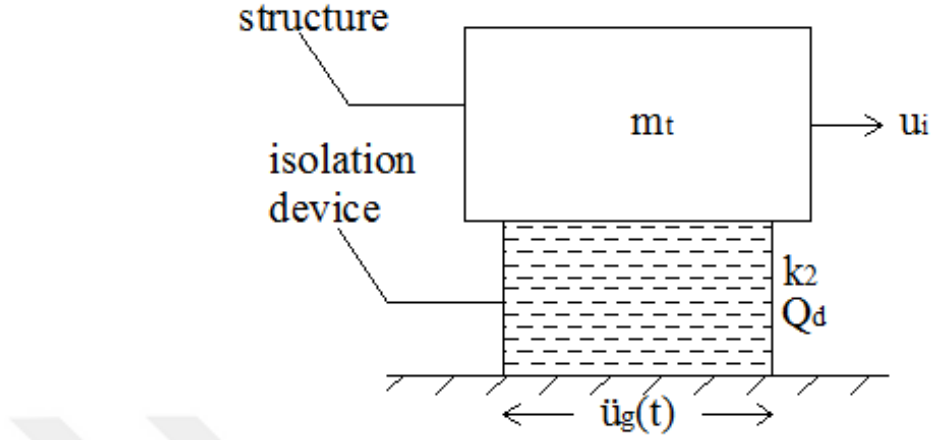
Figure 3.2. Seismic isolation system representation.

The mass is represented by, m_t which describes the total mass above the isolation device. It may consist of the structure mass and the base mass for detailed model. The isolator has bi-linear force-deformation relation which is portrayed by the yield strength Q_d, the post-yield stiffness k_2, and initial stiffness k_1 or yield deformation Δ_y, where Δ_y is;

$$\Delta_y = \frac{Q_d}{k_1 - k_2} \qquad (3.4)$$

The force (F), which can be investigated from the force-deformation relation that is exhibited in Figure 3.1 is formulated by Equation 3.5;

$$F = k_2 u_i + Q z(k_1, u_i, v_i) \qquad (3.5)$$

Isolation deformation is defined as u_i and velocity is defined as v_i in the equations; and z shows the fraction of the yield strength applied.

The deformation of the isolator that supports total mass m_t (*or* weight W), subjected to ground acceleration $\ddot{u}_g(t)$, is governed by the Equation 3.6;

$$\ddot{u}_i(t) + \omega_i{}^2 u_i(t) + SRgz(t, k_1, u_i, v_i) = -\ddot{u}_g(t) \tag{3.6}$$

where; $\omega_i = \sqrt{\frac{k_2}{m_t}}$

Equation 3.6 is solved for a single ground acceleration to obtain the deformation history, $u_i(t)$.

ω_i is a convenient frequency and $T_2 = 2\pi/\omega_i$ b is a suitable period to characterize the isolation system. ω_i is known as the frequency of the isolation and T_2 are generally known as the period of the isolation.

Characteristic strength ratio (SR) which is shortly mentioned in section 3.1, quantifies the strength of the system relative to the system weight (W). SR target ranges provide basis for designing the yield strength of the isolation system.

Nonlinear analyses are performed for each ground motion pairs, for each strength ratio and post-yield stiffness combinations. Then, force-displacement graphs are obtained which help to calculate average displacement in following process of the analysis. An example force-displacement graph is presented in Figure 3.2.

When the average displacement values are calculated, the damping of the system and then the base shear values can be found out.
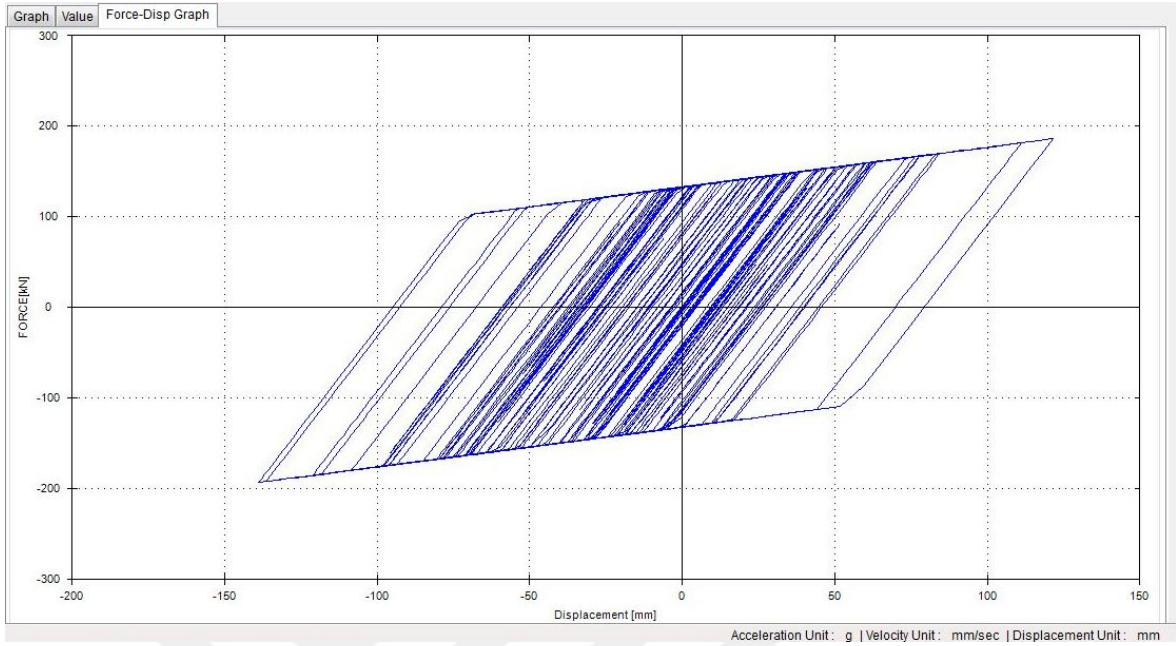
Figure 3.3. A typical bi-linear force-displacement graph which is plotted in PRISM software (PRISM, 2015).

Base shear which is transmitted to superstructure is calculated from the Equation 3.7, in line with the Turkish Building Seismic Design Code (TBSDC, 2018), Chapter 14.

$$V_M = \frac{S_{ae}{}^{DD1}(T_M)W\eta_M}{R} \tag{3.7}$$

Base shear is expressed as V/W on the graphs to make it weight independent. In the Equation 3.7, $S_{ae}^{DD1}(T_M)$ is spectral acceleration for maximum ground motion level at T_M. T_M is the effective vibration period of seismically isolated building at maximum displacement. All indices in Equation 3.7 are given for maximum considered earthquake level, DD1. R is earthquake force reduction factor and it is assigned 1.2 for this study. η is damping scaling coefficient and calculation of it is given in Equation 3.8.

$$\eta = \sqrt{\frac{10}{5 + \xi}} \tag{3.8}$$

ξ is damping ratio and for this study it is calculated as below, Equation 3.9.

$$\xi = \frac{2}{\pi} \left(\frac{\mu}{\mu + \frac{D}{R_c}} \right) \tag{3.9}$$

μ is friction coefficient and it is assumed as 0.05 for this study. D is average displacement which is obtained from nonlinear response analysis. R_c is radius of seismic isolation unit on surface and the formulation of it given in Equation 3.10.

$$R_c = \frac{T^2 g}{4\pi^2} \tag{3.10}$$

g is the acceleration of gravity, T is period.

Although the equations of ξ is written and represented for FPS to define much more parameters above, ξ values are obtained for systems with LRB by using Equation 3.1. The rest of the other equations to find η and V_M remain the same.

$$\xi = \frac{1}{2\pi} \left(\frac{W_d}{FD} \right) \tag{3.11}$$

W_d describes dissipated energy namely, the area inside the force-displacement curve. D represents the displacement value for the seismic isolation unit and F shows the force at isolation unit for corresponding displacement, D.

As a result, the useful contour plot which is shown below is obtained, Figure 3.4. The ADRS graph helps the designer to evaluate the differences between the varying yield level and isolation period to reach the suitable design for interested system.
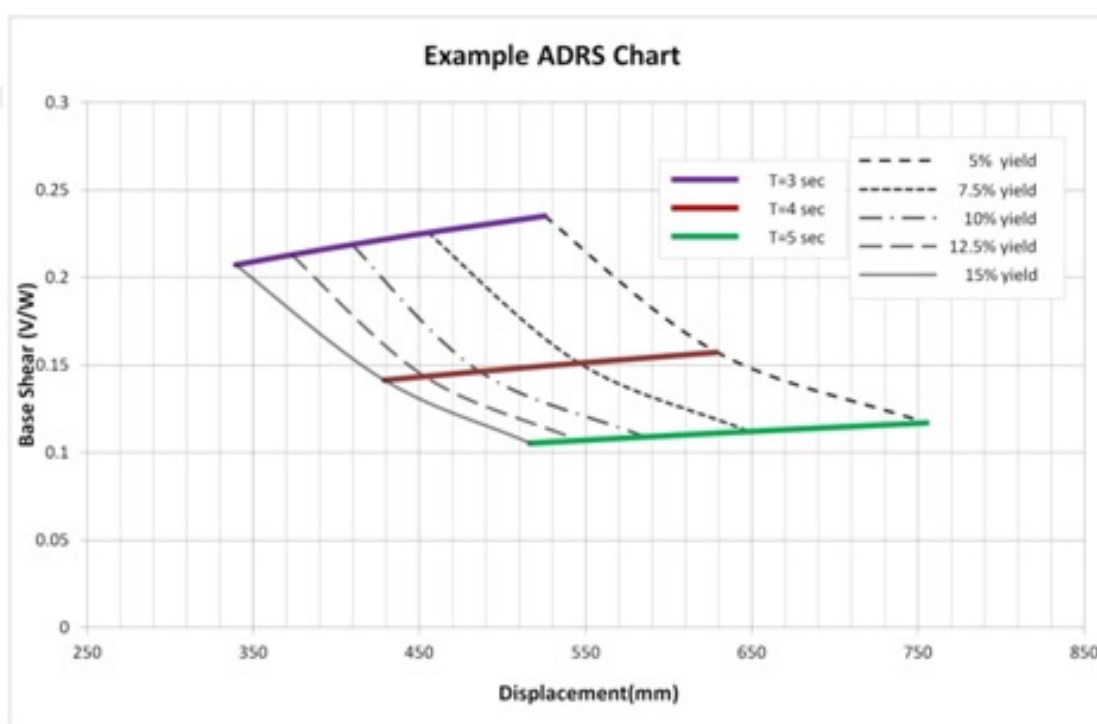
Figure 3.4. Example ADRS plot (horizontal-constant period, T_2, vertical-constant yield level,%).

4. ANALYSES

In the first step, horizontal elastic response spectra are obtained for each design cases. Ground motion pairs are selected by using obtained elastic response spectra. Linear scaling is applied to the selected recordings. The period range is appointed as 1-7 seconds. Hence, average of selected ground motions fits the horizontal elastic spectrum between these periods.

In the second step, nonlinear analyses are performed using the PRISM software (PRISM, 2015) for seismic response analysis of SDOF systems. Input ground motion data are corrected. Then acceleration-time, velocity-time and displacement-time graphs are checked. The bi-linear hysteresis curve model is used to represent nonlinear behavior of a typical seismic isolation system. Analyses are performed for each horizontal component of ground motion pairs for each strength ratio and post-yield stiffness combinations. The flow chart of analysis steps is shown in Figure 4.1.
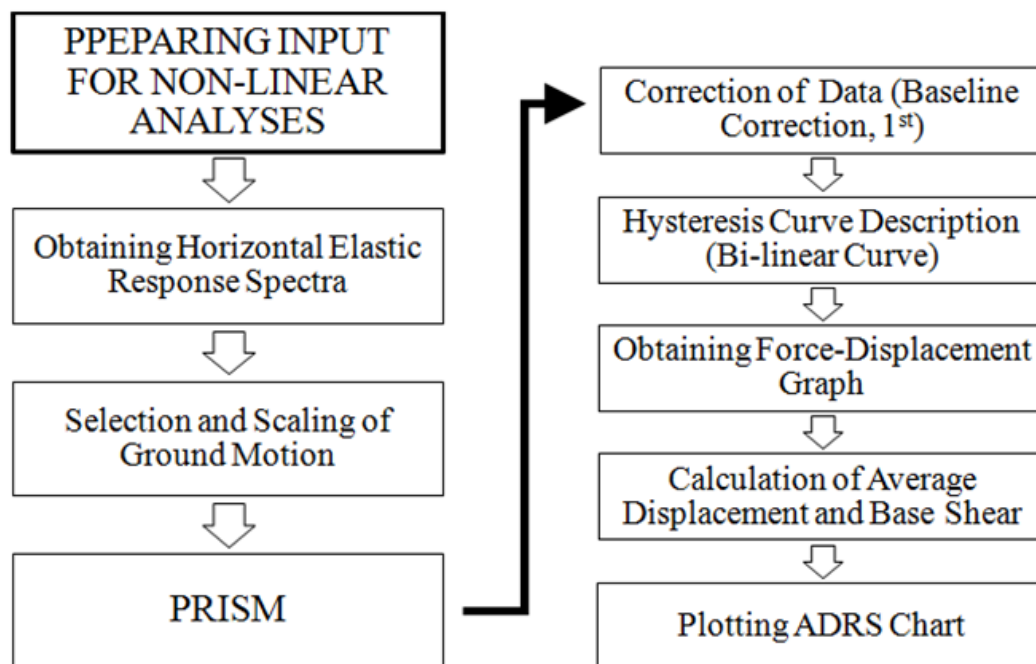
Figure 4.1. Flow chart of the study.

4.1. Strong Ground Motion Recordings: Selection and Scaling of Data

In the first step of analyses, ground motion recordings are obtained and linearly scaled to match horizontal elastic response spectrum of each shaking level and site category couple. Then, 1st order baseline correction is applied to correct data for analyses.

Strong motion recordings are selected and downloaded from Pacific Earthquake Engineering Research (PEER) Center database (NGA-West2, 2015). The recordings are selected following the procedure of updated Turkish Building Seismic Design Code draft version of which has been released in June 2016 and expected to be enforced in the first quarter of 2018.

The magnitude range is assigned as 6.0 to 7.5 and fault mechanism specified as strike slip considering the two major faulting zones exhibiting the high seismic hazard in Turkey, the North Anatolian and the East Anatolian Fault Zone represent strike slip behavior. Distance (R_{jb}) of earthquakes is between 15 km-60 km. 15 km distance is assumed to be the sufficient distance to neglect near field effects. Pulse-like recordings are ignored. Soil types belong to NEHRP C ($(V_s)_{30} = 360$, 760 m/s) and NEHRP D $((V_s)_{30} = 180$, 360 m/s) categories. Recordings are scaled linearly to match the % 5 damped elastic horizontal design spectra which are acquired in line with regulations of Turkey (TBSDC, 2018).

Two locations are chosen which show the typical high hazard and moderate hazard level of Turkey. Shaking levels are obtained from New Probabilistic Seismic Hazard Map of Turkey (TDTH, 2016). Hazard map for S_1, 2475 years return period is shown in Figure 4.2.

Properties of selected two locations (Location-1 and Location-2) are given in tables below, Table 4.1 represents the properties of Location-1 and Table 4.2 represents the properties of Location-2, respectively. Location-1 is 18.5 km and and Location-2 is 17.5 km away from the active faults. The search is made by using 2475 return period.
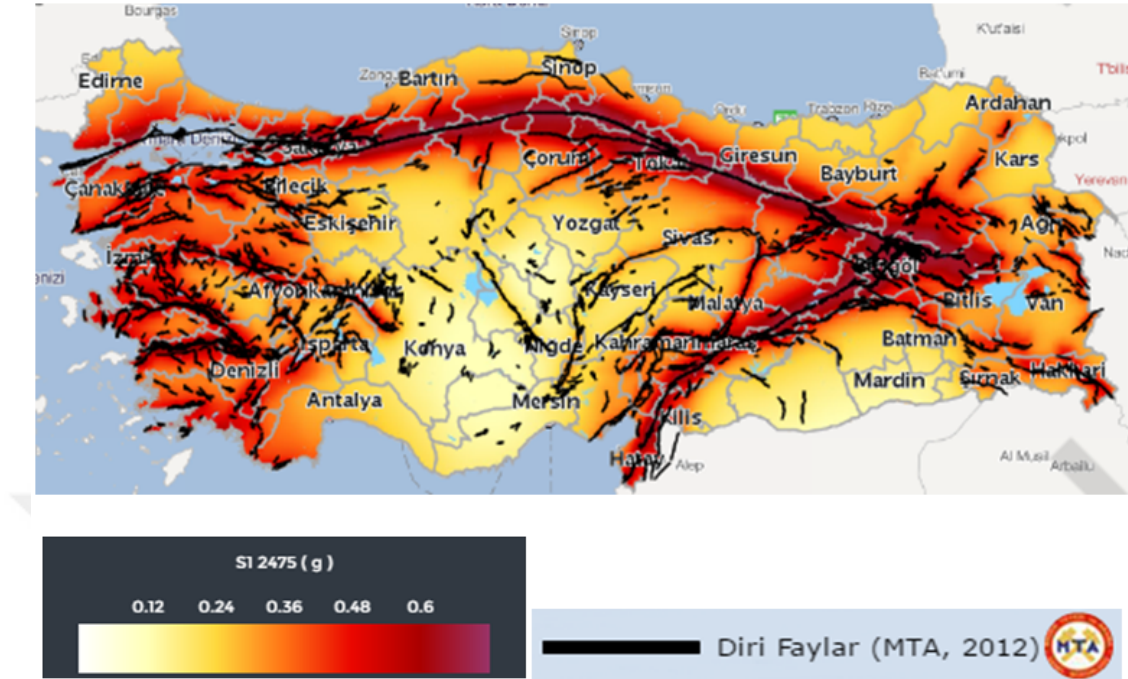
Figure 4.2. Hazard Map for 2475 years return period. (S1 2475) (TDTH, 2016).

Table 4.1. Descriptive parameters of location-1.

Location-1	Coordinates	S_1		S_S		S_{DS}		S_{D1}	
	Latitude Longitude	DD1	DD2	DD1	DD2	DD1	DD2	DD1	DD2
NEHRP C	41.04290 28.85700	0.447	0.256	1.595	0.914	1.914	1.097	0.758	0.434
NEHRP D	41.04290 28.85700	0.447	0.256	1.595	0.914	1.595	1.037	0.936	0.604

Table 4.2. Descriptive parameters of location-2.

Location-2	Coordinates	S_1		S_S		S_{DS}		S_{D1}	
	Latitude Longitude	DD1	DD2	DD1	DD2	DD1	DD2	DD1	DD2
NEHRP C	40.88496 29.28902	0.528	0.292	1.813	1.042	2.176	1.25	0.894	0.504
NEHRP D	40.88496 29.28902	0.528	0.292	1.813	1.042	1.813	1.129	1.076	0.677

The tabulated parameters which are shown above are calculated by using Equation 4.1, 4.2 and 4.3.

$$S_{DS} = S_s F_s \tag{4.1}$$

$$S_{D1} = S_1 \gamma_F F_1 \tag{4.2}$$

$$\gamma_F = 1.2 - 0.02(L_F - 15) \tag{4.3}$$

for $15km < L_F \leq 25km$

In the equations, S_{DS} is short period design spectral acceleration coefficient, S_{D1} is design spectral acceleration coefficient for 1s period and also, γ_F is fault distance coefficient.

S_s represents spectral acceleration coefficient at short period. On the other hand, S_1 is spectral acceleration coefficient for 1 s. period. F_s is site coefficient for short period, F_1 is site coefficient for 1 s. period.

Table 4.3. Fs values given in TBSDC (2018), Section 2.3.3.

Soil Type Fs	Ss≤0.25	Ss=0.50	Ss=0.75	Ss=1.00	Ss=1.25	Ss≥1.50
NEHRP C	1.3	1.3	1.2	1.2	1.2	1.2
NEHRP D	1.6	1.4	1.2	1.1	1.0	1.0

Table 4.4. F1 values given in TBSDC (2018), Section 2.3.3.

Soil Type Fs	Ss≤0.10	Ss=0.20	Ss=0.30	Ss=0.40	Ss=0.50	Ss=0.60
NEHRP C	1.5	1.5	1.5	1.5	1.5	1.4
NEHRP D	2.4	2.2	2.0	1.9	1.8	1.7

Calculated design spectra of all cases for moderate and high hazard levels are shown in Figure 4.3 and 4.4, respectively.
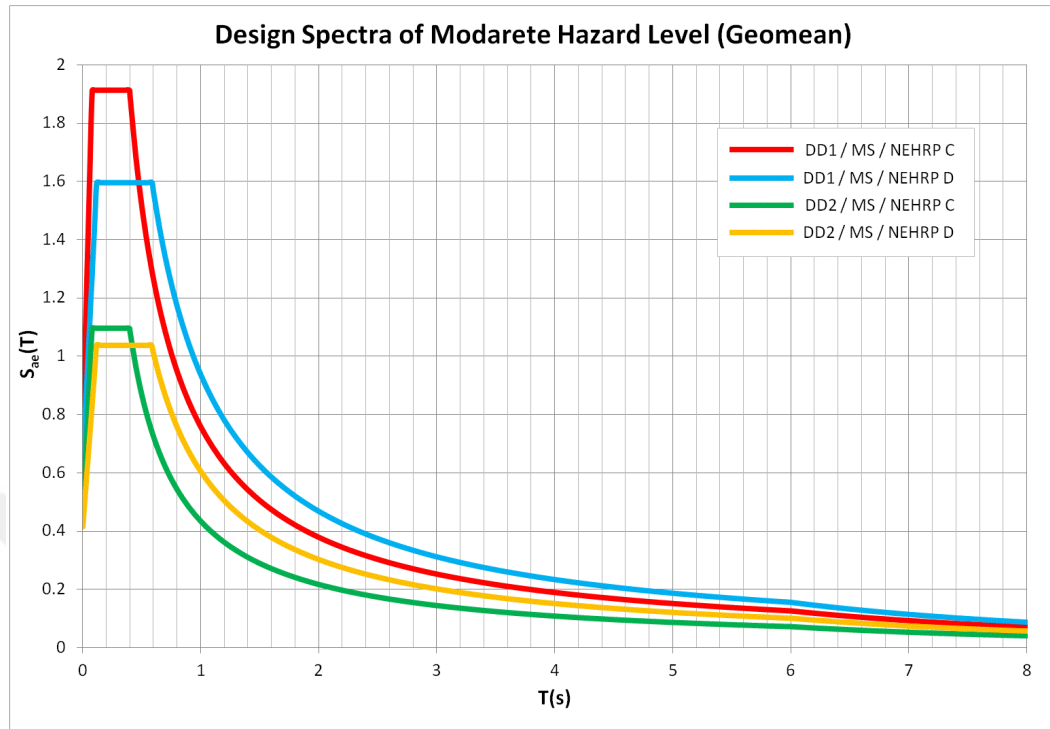
Figure 4.3. Design spectra of moderate hazard level.
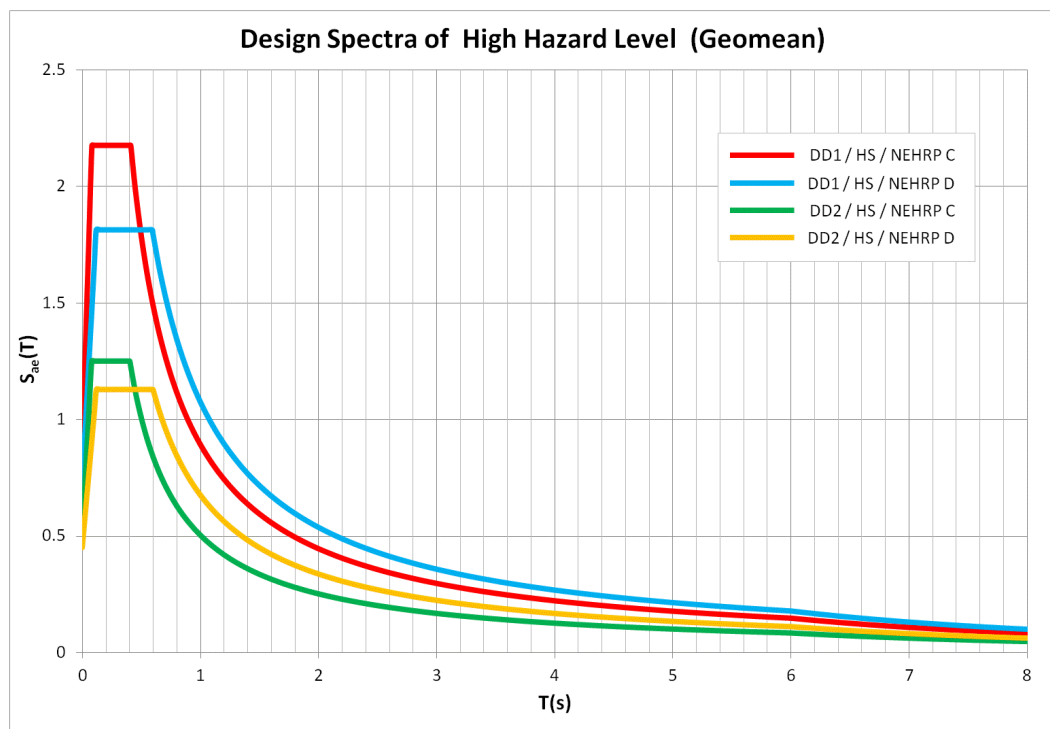
Figure 4.4. Design spectra of high hazard level.

The maximum plato values are observed when the design level is DD1 and soil type is NEHRP C. Conversely, minimum plato values are observed when the design level is DD2 and soil type is NEHRP D. The difference between the maximum and minimum plato value of moderate and hazard levels are 0.874 and 1.05, respectively.

Only two horizontal acceleration components are taken into account. When the recordings are selected, the number of recordings from the same earthquake is limited by three.

Moreover, the same recordings are used with different scale factors if they can be chosen for the each design spectrum of analysis cases of the study. By doing this, the comparison between eight cases are made as possible as with the same recordings. For instance, Case 3 and Case 5 contain the same events with small changes in stations.

Although there are other options in PEER database (NGA-West2, 2015), geomean (geometric mean) spectral ordinate is chosen in analyses. The geomean (GM) of two horizontal acceleration components is calculated as shown in the Equation 4.4 and 4.5.

$$Sa_{GM} = \sqrt{Sa_{FN}Sa_{FP}} \tag{4.4}$$

$$\ln Sa_{GM} = \ln Sa_{FN} + \ln Sa_{FP} \tag{4.5}$$

In the equations above, FN represents the fault normal and FP represents the fault parallel horizontal components of the recording.

By using obtained design spectra of eight cases, eleven selected recordings and their scale factors for geomean analysis cases are presented from Table 4.5 to Table 4.12.

Table 4.5. Selected recordings and scale factors of DD1/Moderate Hazard/NEHRP C.

	Event	Station	Mw	Rjb(km)	Scale Factor
1	Duzce, Turkey 1999	LAMONT 362	7.14	23.41	14.464
2	Hector Mine 1999	ABY	7.13	41.81	2.585
3	Hector Mine 1999	JTN	7.13	50.42	14.359
4	Chi-Chi, Taiwan-04	CHY024	6.20	19.67	5.952
5	Chi-Chi, Taiwan-04	CHY006	6.20	24.58	4.759
6	Chi-Chi, Taiwan-04	CHY029	6.20	25.75	4.747
7	Darfield, New Zealand 2010	HVSCS	7.00	24.36	4.837
8	Darfield, New Zealand 2010	CSHS	7.00	43.60	7.205
9	Darfield, New Zealand 2010	OXZ	7.00	30.63	7.130
10	Landers 1992	FVR	7.28	25.02	8.349
11	El Mayor-Cucapah, Mexico 2010	CISWSHN	7.20	31.79	11.824

Table 4.6. Selected recordings and scale factors of DD1/Moderate Hazard/NEHRP D.

	Event	Station	Mw	Rjb(km)	Scale Factor
1	Imperial Valley-06 1979	DLT	6.53	22.03	2.588
2	Darfield, New Zealand 2010	PPHS	7.00	18.73	1.691
3	Darfield, New Zealand 2010	CHHC	7.00	18.40	2.198
4	Darfield, New Zealand 2010	PRPC	7.00	24.55	2.341
5	El Mayor-Cucapah, Mexico 2010	E11	7.20	15.36	2.062
6	El Mayor-Cucapah, Mexico 2010	TAM	7.20	25.32	2.349
7	Chi-Chi Taiwan-04	CHY101	6.20	21.62	4.098
8	Landers 1992	FHS	7.28	26.84	6.046
9	El Mayor-Cucapah, Mexico 2010	CHI	7.20	18.21	2.588
10	Superstition Hills-02 1987	ICC	6.54	18.20	2.322
11	Victoria, Mexico 1980	CHI	6.33	18.53	3.770

Table 4.7. Selected recordings and scale factors of DD2/Moderate Hazard/NEHRP C.

	Event	Station	Mw	Rjb(km)	Scale Factor
1	Hector Mine 1999	ABY	7.13	41.81	1.480
2	Hector Mine 1999	JTN	7.13	50.42	8.224
3	Hector Mine 1999	29P	7.13	42.06	9.584
4	Darfield, New Zealand 2010	HVS	7.00	24.36	2.770
5	Darfield, New Zealand 2010	CSHS	7.00	43.60	4.126
6	Chi-Chi Taiwan-04 1999	CHY006	6.20	24.58	2.725
7	Chi-Chi Taiwan-04 1999	CHY024	6.20	19.67	3.409
8	Chi-Chi Taiwan-04 1999	CHY029	6.20	25.75	2.719
9	Landers 1992	FVR	7.28	25.02	4.781
10	El Mayor-Cucapah, Mexico 2010	CISWSHN	7.20	31.79	6.772
11	Düzce, Turkey 1999	LAMONT 362	7.14	23.41	8.284

Table 4.8. Selected recordings and scale factors of DD2/Moderate Hazard/NEHRP D.

	Event	Station	Mw	Rjb(km)	Scale Factor
1	Darfield, New Zealand 2010	CCCC	7.00	19.89	1.295
2	Darfield, New Zealand 2010	CHHC	7.00	18.40	1.419
3	Chi-Chi Taiwan-04 1999	CHY101	6.20	21.62	2.645
4	Chi-Chi Taiwan-04 1999	CHY030	6.20	30.46	2.812
5	Superstition Hills-02 1987	ICC	6.54	18.2	1.499
6	Imperial Valley-06 1979	DLT	6.53	22.03	1.670
7	Imperial Valley-06 1979	E12	6.53	17.94	2.770
8	Victoria, Mexico 1980	CHI	6.33	18.53	2.433
9	El Mayor-Cucapah, Mexico 2010	TAM	7.20	25.32	1.516
10	El Mayor-Cucapah, Mexico 2010	CXO	7.20	19.12	1.290
11	El Mayor-Cucapah, Mexico 2010	E11	7.20	15.36	1.330

Table 4.9. Selected recordings and scale factors of DD1/High Hazard/NEHRP C.

	Event	Station	Mw	Rjb(km)	Scale Factor
1	Chi-Chi Taiwan-04 1999	CHY006	6.20	24.58	5.614
2	Chi-Chi Taiwan-04 1999	CHY028	6.20	17.63	7.677
3	Chi-Chi Taiwan-04 1999	CHY024	6.20	19.67	7.021
4	Darfield, New Zealand 2010	OXZ	7.00	30.63	8.411
5	Darfield, New Zealand 2010	CSHS	7.00	43.60	8.500
6	Landers 1992	FVR	7.28	25.02	9.849
7	Hector Mine 1999	ABY	7.13	41.81	3.049
8	Hector Mine 1999	JTN	7.13	50.42	16.939
9	Hector Mine 1999	29P	7.13	42.06	19.741
10	El Mayor-Cucapah, Mexico 2010	CISWSHN	7.20	31.79	13.949
11	Düzce, Turkey 1999	LAMONT 362	7.14	23.41	17.063

Table 4.10. Selected recordings and scale factors of DD1/High Hazard/NEHRP D.

	Event	Station	Mw	Rjb(km)	Scale Factor
1	Darfield, New Zealand 2010	PPHS	7.00	18.73	1.944
2	Darfield, New Zealand 2010	CCCC	7.00	19.89	2.306
3	Darfield, New Zealand 2010	CHHC	7.00	18.40	2.527
4	Chi-Chi Taiwan-04 1999	CHY101	6.20	21.62	4.711
5	Chi-Chi Taiwan-04 1999	CHY030	6.20	30.46	5.009
6	Superstition Hills-02 1987	ICC	6.54	18.20	2.670
7	Imperial Valley-06 1979	DLT	6.53	22.03	2.975
8	Victoria, Mexico 1980	CHI	6.33	18.53	4.334
9	Landers 1992	FHS	7.28	26.84	6.951
10	El Mayor-Cucapah, Mexico 2010	CXO	7.20	19.12	2.298
11	El Mayor-Cucapah, Mexico 2010	E11	7.20	15.36	2.370

Table 4.11. Selected recordings and scale factors of DD2/High Hazard/NEHRP C.

	Event	Station	Mw	Rjb(km)	Scale Factor
1	Hector Mine 1999	ABY	7.13	41.81	1.718
2	Hector Mine 1999	JTN	7.13	50.42	9.546
3	Hector Mine 1999	29P	7.13	42.06	11.125
4	Darfield, New Zealand 2010	HVS	7.00	24.36	3.215
5	Darfield, New Zealand 2010	CSHS	7.00	43.60	4.790
6	Darfield, New Zealand 2010	OXZ	7.00	30.63	4.740
7	Chi-Chi Taiwan-04 1999	CHY006	6.20	24.58	3.164
8	Chi-Chi Taiwan-04 1999	CHY028	6.20	17.63	4.327
9	Chi-Chi Taiwan-04 1999	CHY029	6.20	25.75	3.156
10	El Mayor-Cucapah, Mexico 2010	CISWSHN	7.20	31.79	7.861
11	Düzce, Turkey 1999	LAMONT 362	7.14	23.41	9.616

Table 4.12. Selected recordings and scale factors of DD2/High Hazard/NEHRP D.

	Event	Station	Mw	Rjb(km)	Scale Factor
1	Darfield, New Zealand 2010	PRPC	7.00	24.55	1.693
2	Darfield, New Zealand 2010	CHHC	7.00	18.40	1.590
3	Darfield, New Zealand 2010	PPHS	7.00	18.73	1.223
4	Chi-Chi Taiwan-04 1999	CHY101	6.20	21.62	2.964
5	Chi-Chi Taiwan-04 1999	CHY030	6.20	30.46	3.152
6	Superstition Hills-02 1987	ICC	6.54	18.20	1.680
7	Imperial Valley-06 1979	DLT	6.53	22.03	1.872
8	Imperial Valley-06 1979	E12	6.53	17.94	3.105
9	Victoria, Mexico 1980	CHI	6.33	18.53	2.727
10	El Mayor-Cucapah, Mexico 2010	TAM	7.20	25.32	1.699
11	El Mayor-Cucapah, Mexico 2010	E11	7.20	15.36	1.491

4.2. Design Hazard Levels

Maximum Considered Earthquake (DD1) and Design Basis Earthquake (DD2) design levels are considered in the study. In order to select the appropriate hazard levels, probabilistic hazard results of Turkey (TDTH, 2016) in terms of Spectral Acceleration at 1 second period (S_1) have been investigated. For the reference site condition, maximum S_1 at DD1 hazard level is 1.4 g on the active faults (R=0) and sharply decreases to 0.6 g at approximately 15-20 km away from the fault line. It further decreases to 0.4 g at 45-50 km epicentral distance. Hence calculations are performed between 0.4 g and 0.6 g, S_1 range by dividing this range into two as moderate hazard (0.4g≤S_1(DD1)<0.5g) and high hazard (0.5g≤S_1(DD1)<0.6g). Average values of these ranges have been used for calculating the elastic response spectra. Corresponding mean S_1 at DD2 hazard level is 0.25 g for moderate hazard and 0.30 g for high hazard ranges. Combination of ground motion and isolation system parameters is exhibited in Table 4.13 and Table 4.14.

Elastic response spectra of selected and scaled recordings are shown below to show dispersion of the selected recordings according to related elastic response spectra (Figure 4.5-4.12). The bold lines which represent the mean line of selected recordings match the elastic response spectra of each case in the interested period range which is 1-7 seconds.

Table 4.13. Combination of ground motions.

Categories	Values
Design Levels	Maximum Considered Earthquake (DD1),
	Design Basis Earthquake (DD2)
Hazard Levels	0.4g≤S_1(DD1)<0.5g,
	0.5g≤S_1(DD1)<0.6g
Site Categories	NEHRP C, NEHRP

Figure 4.5. Target acceleration spectrum and spectra for scaled ground motions for
DD1 / Moderate Hazard / NEHRP C (Case 1).

Figure 4.6. Target acceleration spectrum and spectra for scaled ground motions for
DD1 / Moderate Hazard / NEHRP D (Case 2).

Figure 4.7. Target acceleration spectrum and spectra for scaled ground motions for DD2 / Moderate Hazard / NEHRP C (Case 3).

Figure 4.8. Target acceleration spectrum and spectra for scaled ground motions for DD2 / Moderate Hazard / NEHRP D (Case 4).

Figure 4.9. Target acceleration spectrum and spectra for scaled ground motions for
DD1 / High Hazard / NEHRP C (Case 5).

Figure 4.10. Target acceleration spectrum and spectra for scaled ground motions for
DD1 / High Hazard / NEHRP D (Case 6).
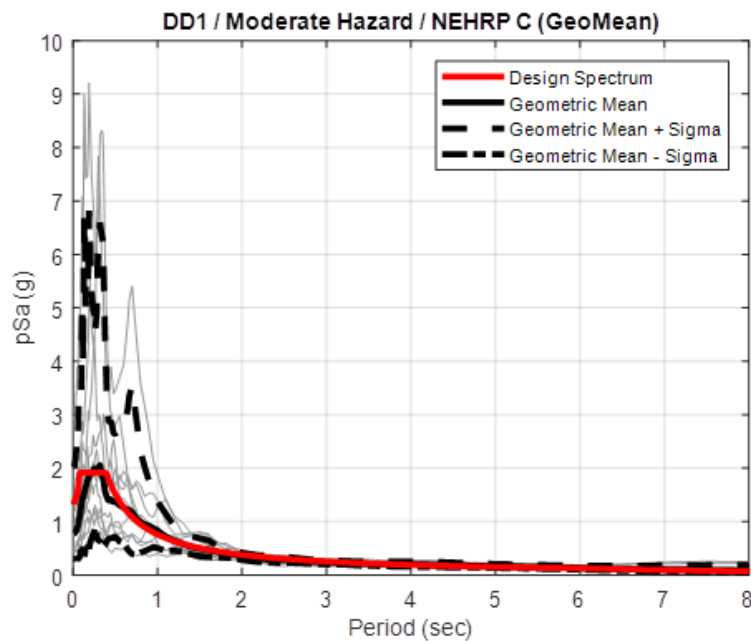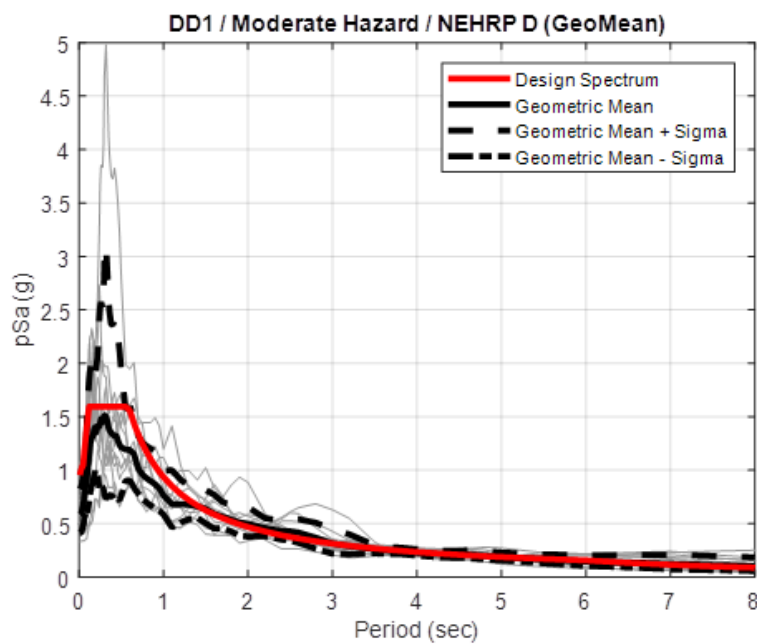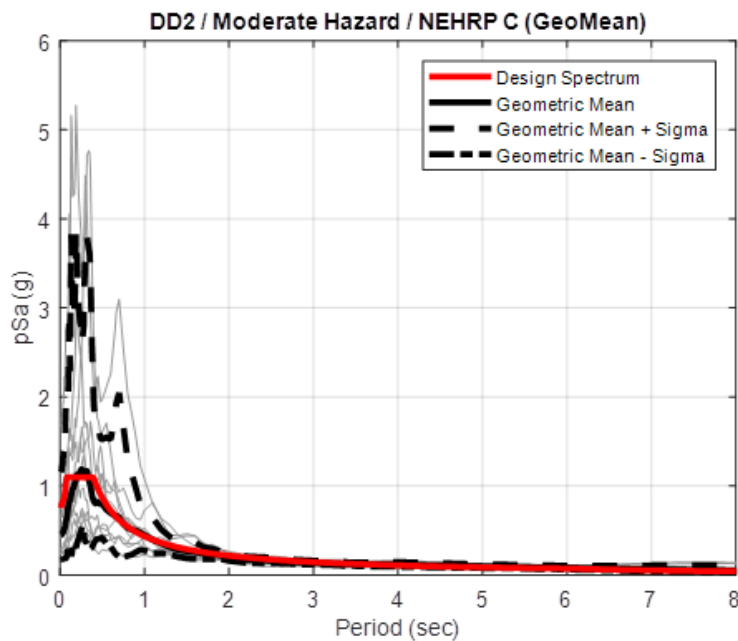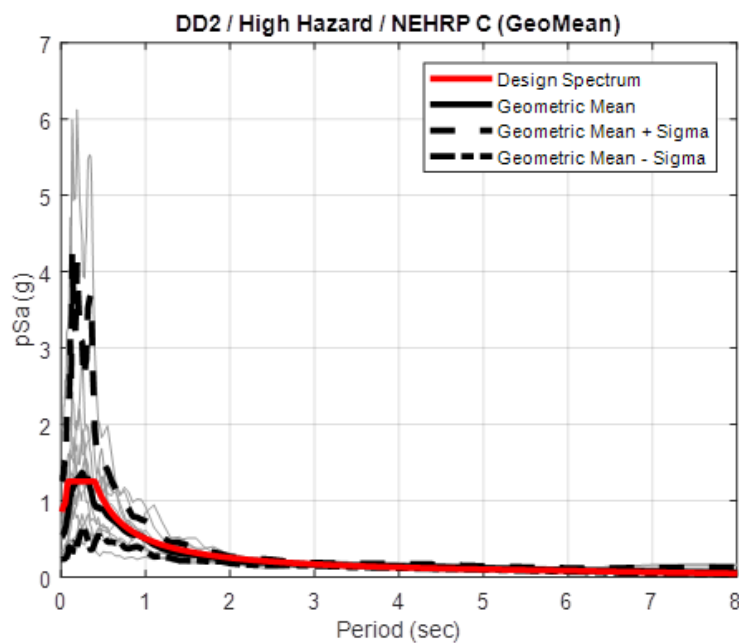
Figure 4.11. Target acceleration spectrum and spectra for scaled ground motions for
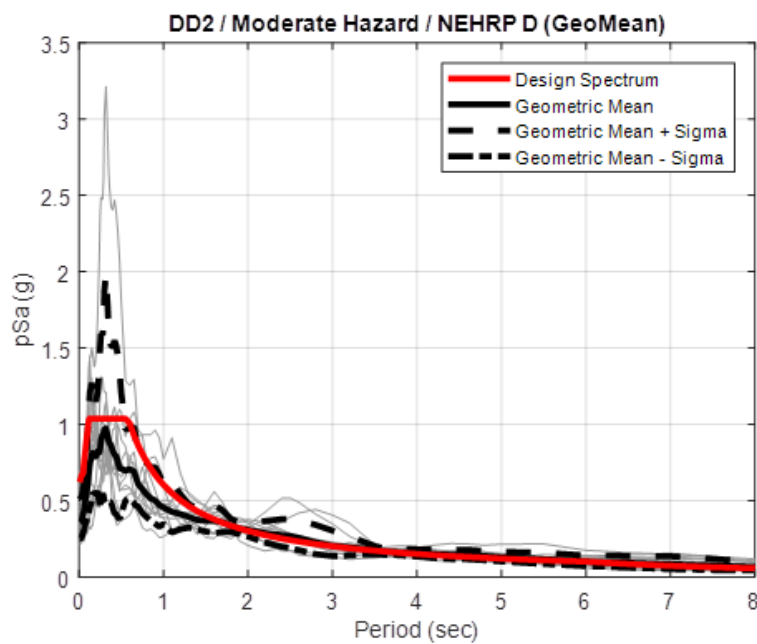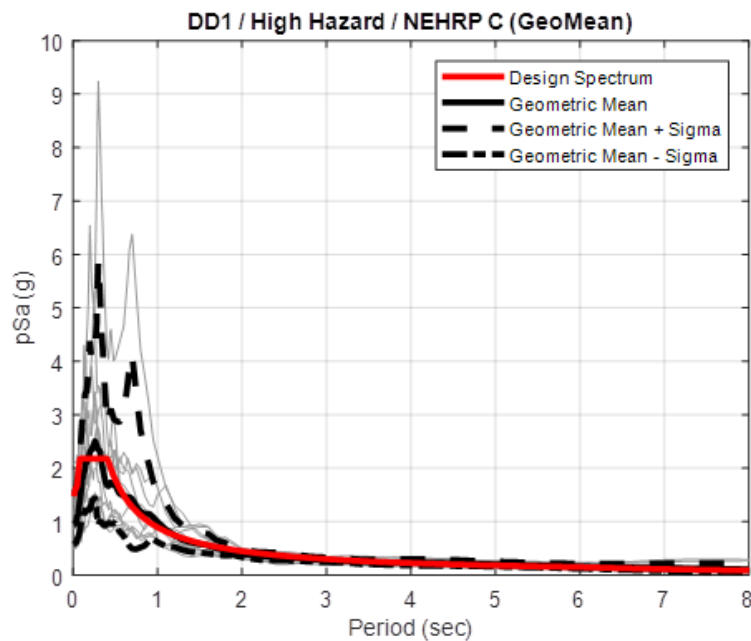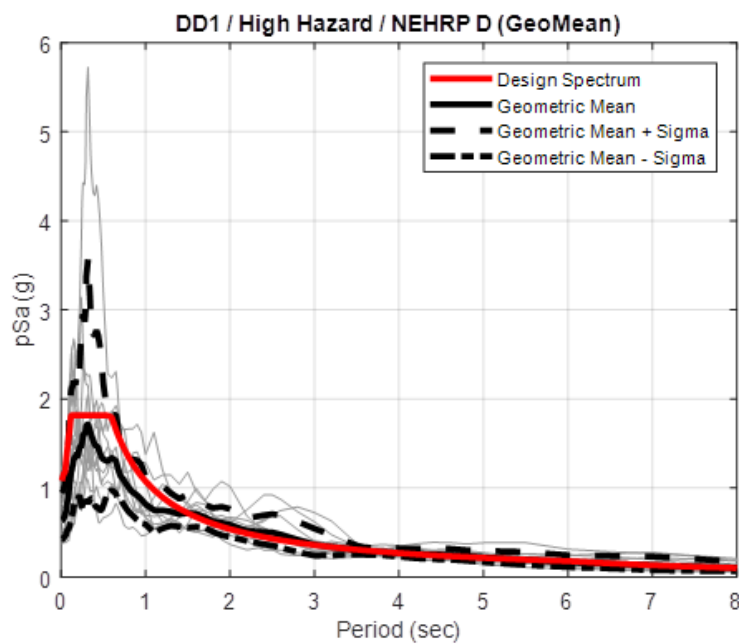DD2 / High Hazard / NEHRP C (Case 7).
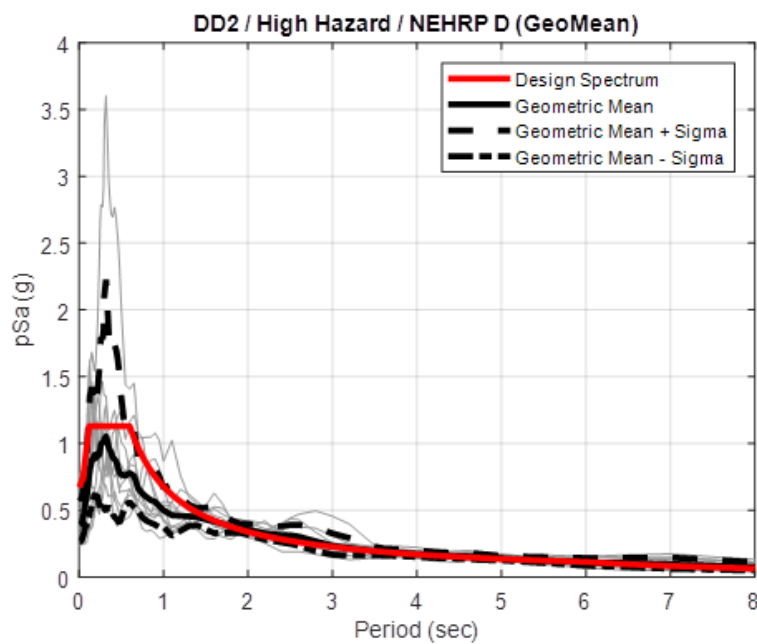
Figure 4.12. Target acceleration spectrum and spectra for scaled ground motions for
DD2 / High Hazard / NEHRP D (Case 8).

4.3. Nonlinear Analysis

Nonlinear analysis of the isolator has been performed using freely available software. (PRISM, 2015). Bi-linear curve description is done by entering T_2, SR and α in PRISM software for seismic response analysis of SDOF systems.

The calculation of post-to-pre yield stiffness ratio (α) are done by the Equation 3.1, the second slope period of vibration (T_2) and strength ratio (SR) are calculated by Equation 3.2 and Equation 3.3, respectively. Combination of seismic isolation parameters are given in Table 4.14.

Table 4.14. Combination of seismic isolation system parameters.

Categories	Values
Post Elastic Periods (s)	2, 2.5, 3, 3.5, 4.0, 5.0
Yield Levels (W%)	5.0, 7.5, 10.0, 12.5, 15.0

Input ground motion data are corrected by using 1st order baseline correction. Afterwards, acceleration-time, velocity-time and displacement-time histories are obtained for both two horizontal component of ground motion and the graphs are checked to see whether there is an irregularity on them or not.

A total 5280 nonlinear analyses are performed and ADRS are obtained for eleven ground motion pairs, with six post elastic periods ($T_2 = 2$, 2.5, 3, 3.5, 4, 5 s) and five yield level values (5%, 7.5%, 10%, 12.5%, 15% of W) defined.

Square root of the sum of the squares (SRSS) of two response displacements at period t_{dmax}, which is the period corresponding to the largest response displacement in a horizontal direction, is calculated. The largest of the SRSS is considered as the maximum response displacement of the system excited with the scaled ground motion pair and averages of 11 ground motions pair are calculated. Base shear which is transferred to superstructure is calculated using Equation 3.4, in line with the TBSDC (2018).

5. RESULTS

Results of the analyses are given in order as seen in below chart, Figure 5.1. Firstly, ADRS graphs are explained one by one. Then, effects of soil type, design level and hazard level change are compared.
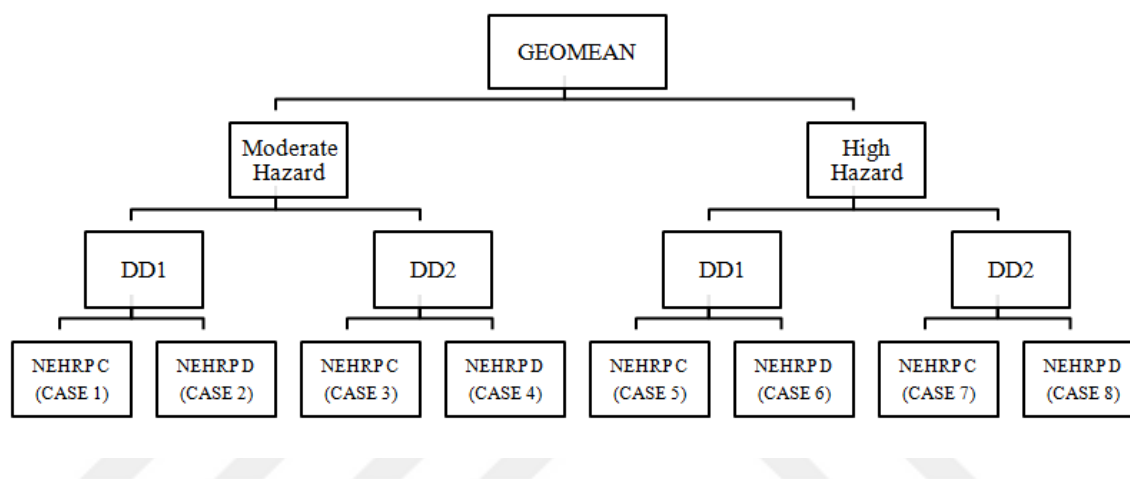
Figure 5.1. Schematic description of analyses cases.

The analyses results are represented as eight ADRS graphs which are shown in the following pages, in Figure 5.2-5.9. These are;

Case-1: DD1/Moderate hazard/NEHRP C,

Case-2: DD1/Moderate hazard/NEHRP D,

Case-3: DD2/Moderate hazard/NEHRP C,

Case-4: DD2/Moderate hazard/NEHRP D,

Case-5: DD1/High hazard/NEHRP C,

Case-6: DD1/High hazard/NEHRP D,

Case-7: DD2/High hazard/NEHRP C,

Case-8: DD2/High hazard/NEHRP D for scaled recordings according to geomean spectral ordinate.

As it is expected, for the given shortest period (T=2 s) and given smallest yield ratio (5% W) base shear ratio of the systems has its highest value and vice versa. Besides, for the given shortest period (T=2 s) and greatest yield ratio (15%W) displacements are the smallest and for the longest period (T=5 s) and smallest yield ratio (5% W) displacement values are the highest in all cases. Higher structural periods enable the structure to have a higher displacement capacity.

Case 3 and Case 6 show the two extreme results of the system and worth comparing. Case 6 shows the response of the system under DD1, high hazard level and soft soil conditions (Figure 5.7). Maximum base shear is 0.4 (V/W). Displacement range is between 217 mm and 755 mm. Case 3, on the contrary, shows the response of the system under DD2, moderate hazard level and stiff soil condition (Figure 5.4). Maximum base shear ratio is around 0.12 (V/W) and displacement range is limited to 92 mm - 237 mm. There is a similar proportional reduction in minimum base shears, from 0.1 (V/W) to 0.035 (V/W). There is an approximately three times difference in maximum and minimum base shears of Case 6 and Case 3 (Figure 5.7 and Figure 5.4). The maximum displacement value of Case 3 is nearly equal to the minimum displacement of Case 6. The effect of yield levels which are above 10% is not significant on ADRS chart in Case 3 (Figure 5.4) when the period is 3 s.

For moderate hazard conditions, DD1 maximum and minimum base shear values are approximately two times greater than DD2. (There is an from 1.76 and 2.08 times difference between the base shear values.)

The figures of Case 1, Case 2, Case 3 and Case 4 are exhibited then the responses are represented in tables.
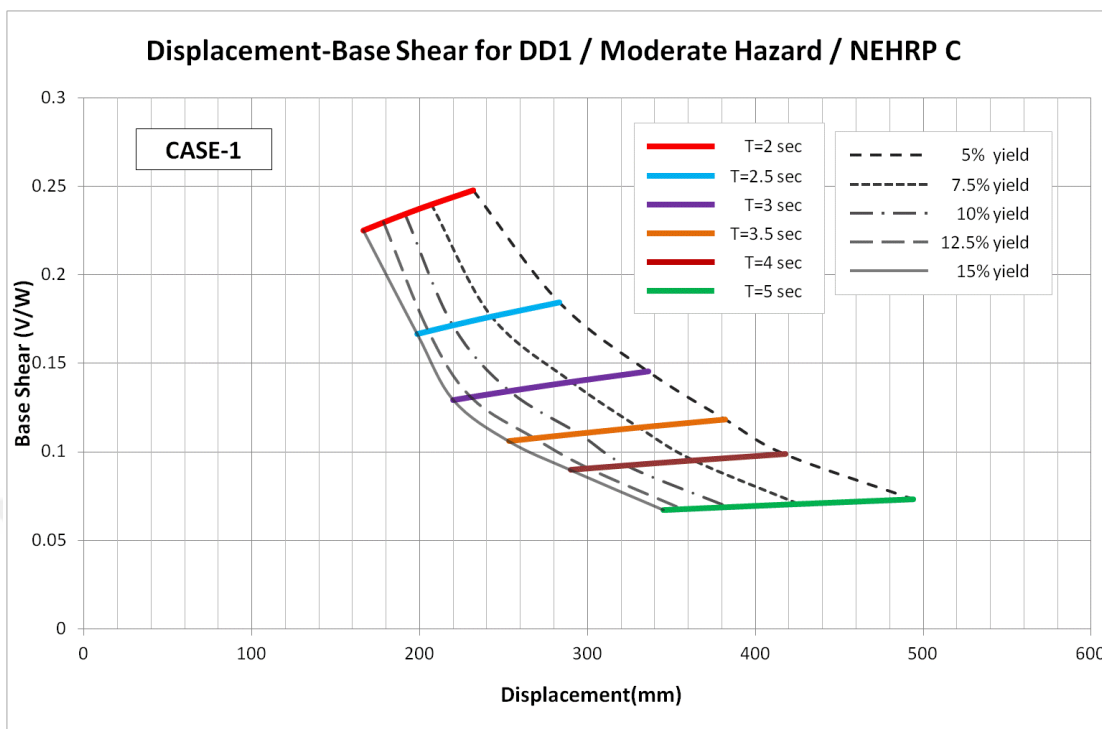
Figure 5.2. Case 1: DD1 / Moderate hazard / NEHRP C.
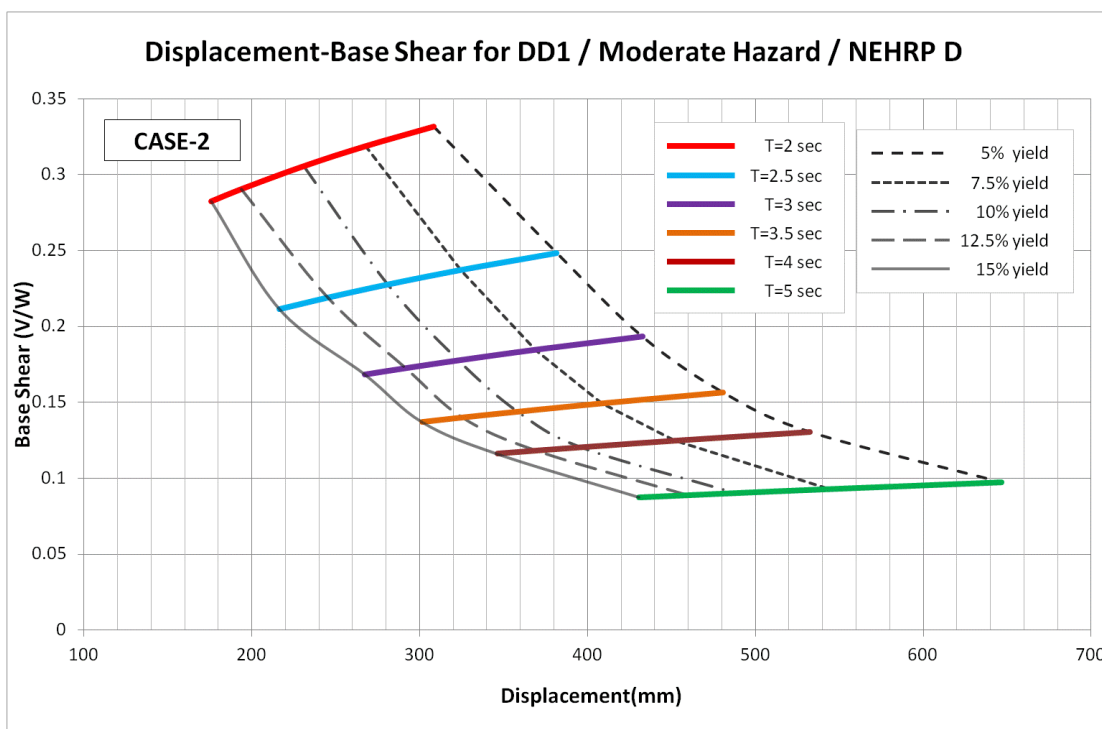
Figure 5.3. Case 2: DD1 / Moderate hazard / NEHRP D.
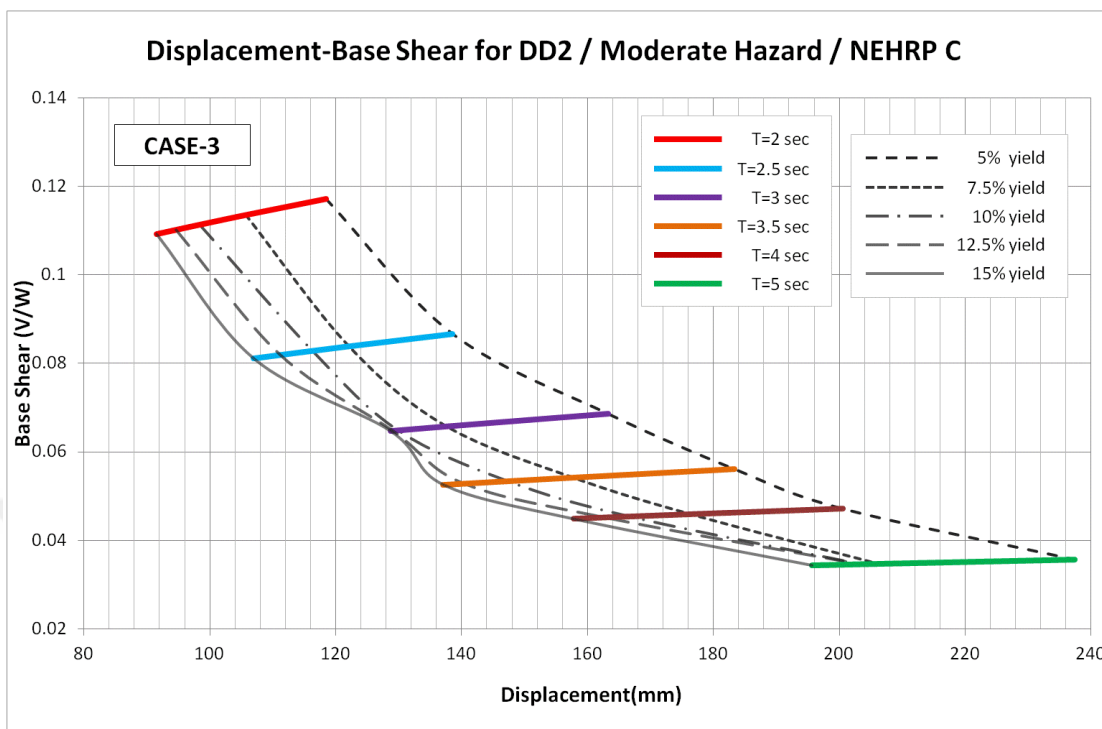
Figure 5.4. Case 3: DD2 / Moderate hazard / NEHRP C.
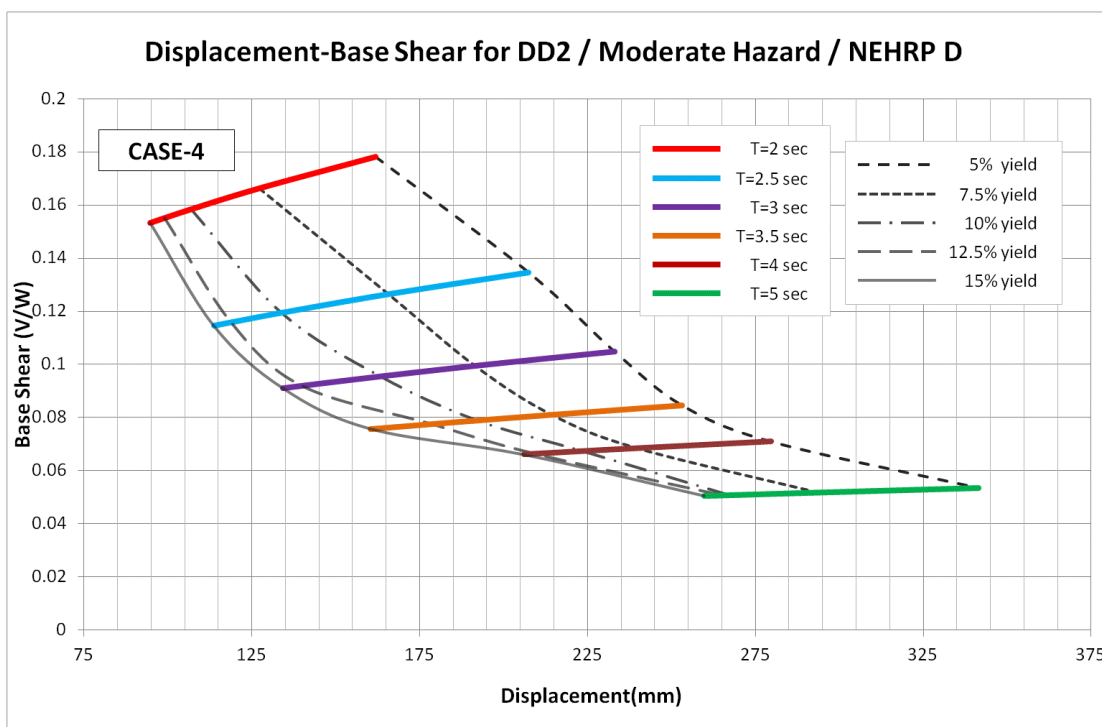
Figure 5.5. Case 4: DD2 / Moderate hazard / NEHRP D.

Table 5.1. Displacement values at each period and strength ratio of Case 1.

Displacements (mm)						
SR/T	**2**	**2.5**	**3**	**3.5**	**4**	**5**
5%	231.97	283.05	336.02	381.92	417.72	494.03
7.5%	206.90	242.57	290.20	330.40	363.28	425.35
10%	191.10	219.51	253.49	294.80	323.41	384.10
12.5%	178.51	205.17	230.54	268.70	301.23	356.69
15%	166.40	198.43	220.00	253.18	290.08	345.14

Table 5.2. Base shear values at each period and strength ratio of Case 1.

Base Shear (V/W)						
SR/T	**2**	**2.5**	**3**	**3.5**	**4**	**5**
5%	0.248	0.185	0.146	0.119	0.099	0.073
7.5%	0.240	0.177	0.140	0.114	0.095	0.071
10%	0.234	0.172	0.134	0.110	0.092	0.069
12.5%	0.230	0.168	0.131	0.108	0.091	0.068
15%	0.225	0.167	0.129	0.106	0.090	0.067

Table 5.3. Displacement values at each period and strength ratio of Case 2.

Displacements (mm)						
SR/T	**2**	**2.5**	**3**	**3.5**	**4**	**5**
5%	308.44	381.60	432.60	480.88	532.39	646.46
7.5%	267.71	324.70	368.92	408.21	452.13	543.43
10%	230.93	281.06	323.07	358.48	396.65	488.02
12.5%	193.94	245.65	291.80	325.65	370.35	459.70
15%	175.65	216.58	267.22	301.34	346.60	430.85

Table 5.4. Base shear values at each period and strength ratio of Case 2.

Base Shear (V/W)						
SR/T	2	2.5	3	3.5	4	5
5%	0.331	0.248	0.193	0.156	0.131	0.097
7.5%	0.319	0.237	0.185	0.149	0.125	0.093
10%	0.306	0.228	0.178	0.144	0.120	0.090
12.5%	0.291	0.219	0.173	0.140	0.118	0.089
15%	0.283	0.211	0.169	0.137	0.116	0.088

Table 5.5. Displacement values at each period and strength ratio of Case 3.

Displacements (mm)						
SR/T	2	2.5	3	3.5	4	5
5%	118.47	138.58	163.31	183.33	200.50	237.41
7.5%	105.74	122.14	137.60	157.74	176.54	206.30
10%	98.44	116.35	129.88	147.26	166.70	203.21
12.5%	94.64	111.21	129.00	140.23	162.67	203.06
15%	91.53	106.96	128.67	137.08	157.84	195.66

Table 5.6. Base shear values at each period and strength ratio of Case 3.

Base Shear (V/W)						
SR/T	2	2.5	3	3.5	4	5
5%	0.117	0.087	0.069	0.056	0.047	0.036
7.5%	0.114	0.084	0.066	0.054	0.046	0.035
10%	0.111	0.083	0.065	0.053	0.045	0.035
12.5%	0.110	0.082	0.065	0.053	0.045	0.035
15%	0.109	0.081	0.065	0.053	0.045	0.034

Lastly, the tables for Case 4 are given below:

Table 5.7. Displacement values at each period and strength ratio of Case 4.

Displacements (mm)						
SR/T	2	2.5	3	3.5	4	5
5%	161.80	207.36	233.07	253.17	279.72	341.44
7.5%	127.27	165.71	191.58	214.30	239.95	293.40
10%	106.88	133.80	163.38	192.11	223.81	267.27
12.5%	98.99	118.76	139.86	178.28	209.47	264.85
15%	94.74	113.68	134.30	160.43	206.15	259.86

Table 5.8. Base shear values at each period and strength ratio of Case 4.

Base Shear (V/W)						
SR/T	2	2.5	3	3.5	4	5
5%	0.178	0.135	0.105	0.085	0.071	0.054
7.5%	0.166	0.127	0.099	0.081	0.068	0.052
10%	0.158	0.119	0.095	0.079	0.067	0.051
12.5%	0.155	0.116	0.092	0.078	0.066	0.051
15%	0.153	0.115	0.091	0.076	0.066	0.051

Figure 5.2 shows the responses of the system under DD1, moderate hazard level and stiff soil condition (Case 1). Maximum base shear is around 0.25 (V/W). Displacements are between 166 mm an 494 mm, where as Figure 5.3 shows the responses of the system under DD1, moderate hazard level but soft soil condition (Case 2). Maximum base shear is 0.33 (V/W). Displacement range is between 176 mm and 647 mm.

Comparison of Figure 5.2 and Figure 5.3 portrays the isolator response under different soil conditions. When they are compared, the effect of yield level increases in higher periods for stiffer soil. Hence, the horizontal lines which show the displacement

range for the same period lengthen in higher periods. On the other hand, effect of yield levels cause uniform change in all periods for softer soil type.

In a similar way, Figure 5.4 (Case 3) and Figure 5.5 (Case 4) presents the response of the system under DD2, moderate hazard level ground motion suites recorded on stiff and soft soil conditions, respectively. Maximum base shear is 0.178 (V/W), displacement range is between 95 mm and 341 mm in Figure 5.5.

When Figure 5.4 and Figure 5.5 are compared, for DD2 level, the effect of soil type on minimum displacement is negligible because there is only 3 mm difference between the minimum displacement value of soft and stiff soil.

Figure 5.6 and Figure 5.7 portray the change in the response of the system when the soil type switches from NEHRP D to NEHRP C. Figure 5.6 shows the responses of the system under DD1, high hazard level and stiff soil condition (Case 5). Maximum base shear ratio is 0.31 (V/W). Displacement range is between 226 mm and 595 mm. Figure 5.7 shows the responses of the system under DD1, high hazard level and soft soil condition (Case 6). Maximum base shear ratio is 0.4 (V/W). Displacement range is between 217 mm and 755 mm. The average displacement range is 190 mm between 2.5 and 4 seconds for Case 6. When the soil becomes stiffer maximum base shear ratio is reduced about one fourth and max displacement is reduced about 15 cm. Maximum displacement is reduced by 170 mm by the different soil type property. There is not significant difference between minimum displacement responses of Case 5 and Case 6.

In Case 5, the effect of yield level diminishes in low period ranges and consequently the line which represents displacement range is shortening in high base shear values. On the other hand, all periods are highly affected by yield level in Case 6. Consequently, at soft soil, seismic isolation systems with high fundamental period necessitate very high displacement capability which might not be feasible in terms of seismic isolator production. In this case, designers may reduce the period of structure for a better performance.
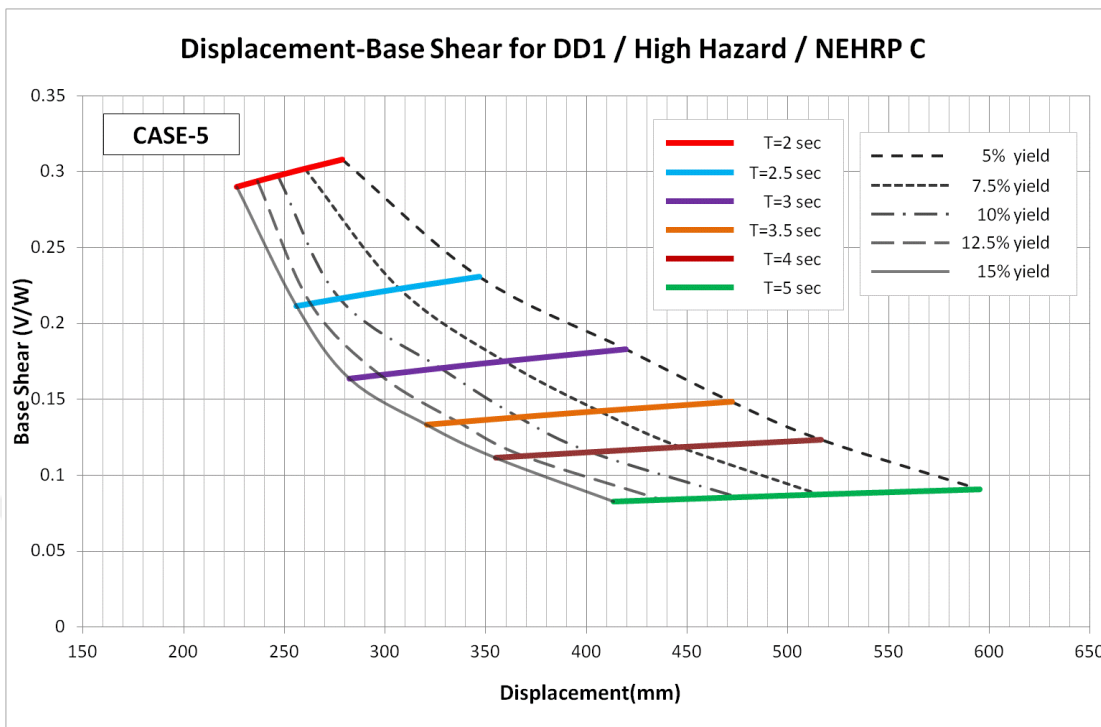
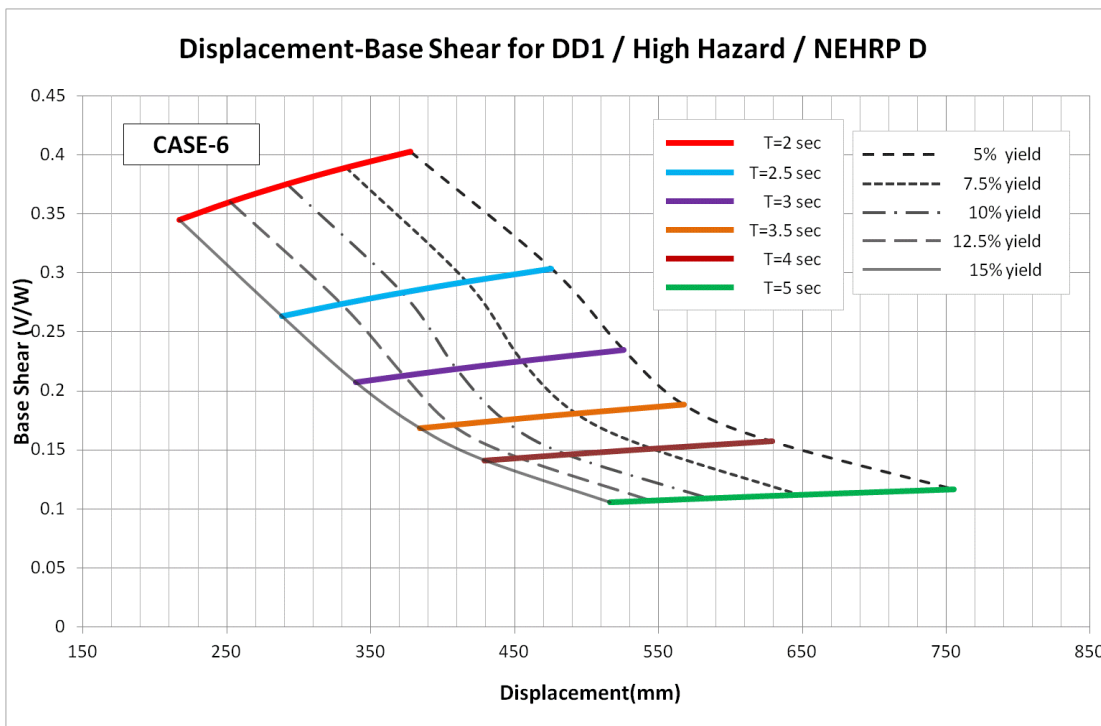Figure 5.6. Case 5: DD1 / High hazard / NEHRP C.

Figure 5.7. Case 6: DD1 / High hazard / NEHRP D.
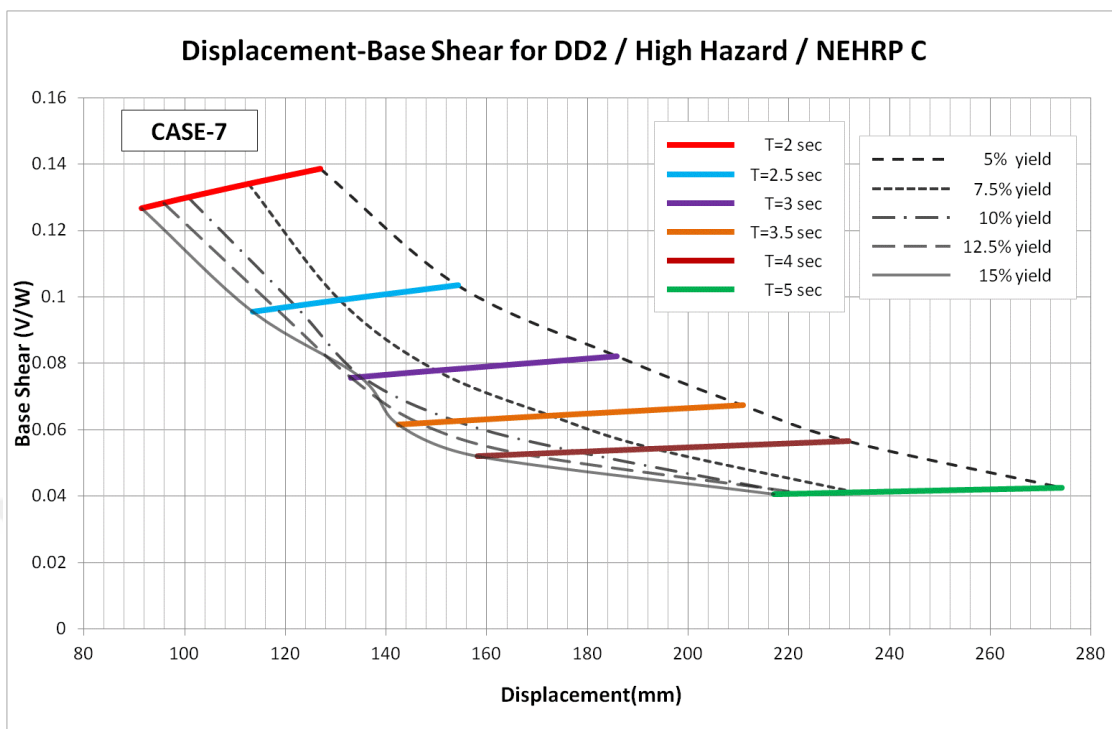
Figure 5.8. Case 7: DD2 / High hazard / NEHRP C.
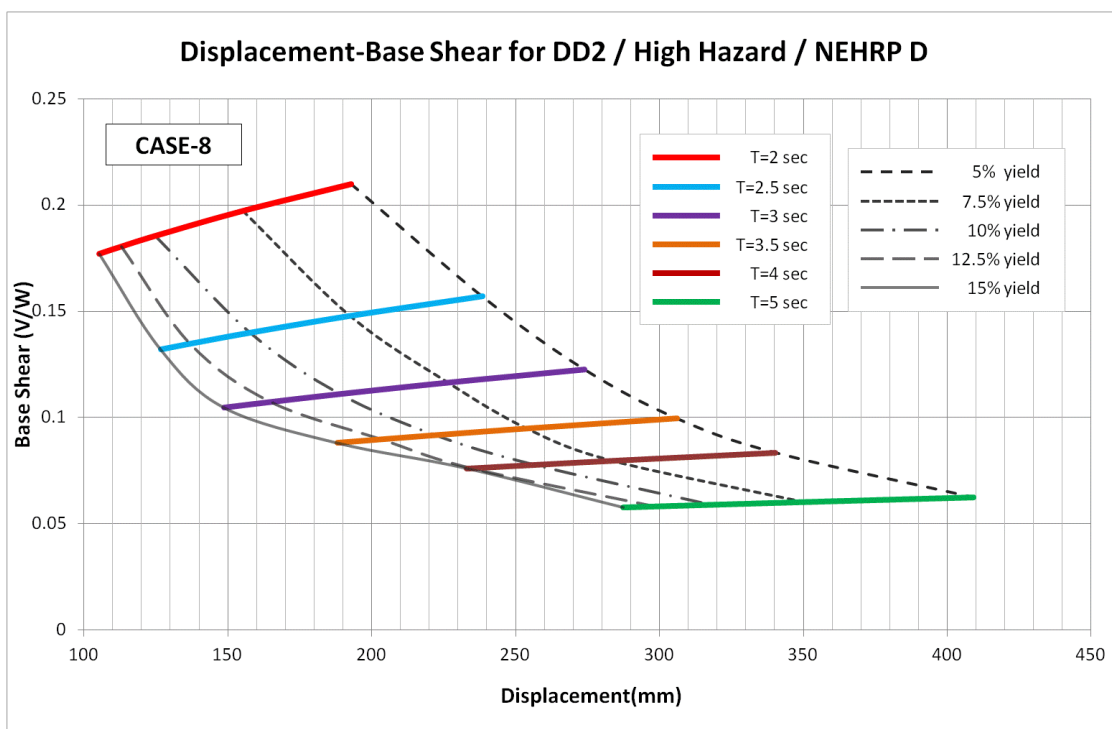
Figure 5.9. Case 8: DD2 / High hazard / NEHRP D.

Table 5.9. Displacement values at each period and strength ratio of Case 5.

Displacements (mm)						
SR/T	2	2.5	3	3.5	4	5
5%	278.82	346.62	419.66	472.05	516.53	595.22
7.5%	260.30	307.21	359.52	406.43	446.64	515.41
10%	246.67	277.30	327.69	366.34	402.21	475.05
12.5%	236.69	262.92	297.63	336.14	368.52	436.45
15%	226.23	255.94	282.44	320.66	354.85	413.26

Table 5.10. Base shear values at each period and strength ratio of Case 5.

Base Shear (V/W)						
SR/T	2	2.5	3	3.5	4	5
5%	0.308	0.231	0.183	0.149	0.124	0.091
7.5%	0.302	0.223	0.175	0.142	0.119	0.088
10%	0.297	0.216	0.170	0.138	0.115	0.086
12.5%	0.294	0.213	0.166	0.135	0.113	0.084
15%	0.290	0.212	0.163	0.133	0.112	0.083

Table 5.11. Displacement values at each period and strength ratio of Case 6.

Displacements (mm)						
SR/T	2	2.5	3	3.5	4	5
5%	377.56	475.54	525.57	567.45	628.84	755.25
7.5%	332.89	416.59	455.28	492.85	546.03	648.61
10%	291.62	371.60	409.47	442.53	486.19	585.51
12.5%	252.33	329.54	373.17	406.43	453.06	545.21
15%	216.86	288.14	339.58	383.89	429.02	516.48

Table 5.12. Base shear values at each period and strength ratio of Case 6.

Base Shear (V/W)						
SR/T	2	2.5	3	3.5	4	5
5%	0.402	0.304	0.235	0.188	0.157	0.117
7.5%	0.389	0.293	0.226	0.181	0.151	0.112
10%	0.375	0.283	0.219	0.176	0.146	0.109
12.5%	0.360	0.274	0.213	0.171	0.143	0.107
15%	0.345	0.264	0.207	0.169	0.141	0.105

Table 5.13. Displacement values at each period and strength ratio of Case 7.

Displacements (mm)						
SR/T	2	2.5	3	3.5	4	5
5%	126.99	154.29	185.76	210.87	231.82	274.17
7.5%	112.72	130.83	149.86	172.77	193.23	233.00
10%	100.77	122.07	135.25	153.96	178.06	220.88
12.5%	95.87	118.20	133.04	146.76	167.34	222.94
15%	91.41	113.53	134.80	142.46	158.10	217.08

Table 5.14. Base shear values at each period and strength ratio of Case 7.

Base Shear (V/W)						
SR/T	2	2.5	3	3.5	4	5
5%	0.139	0.103	0.082	0.067	0.057	0.043
7.5%	0.134	0.099	0.078	0.064	0.054	0.041
10%	0.130	0.097	0.076	0.063	0.053	0.041
12.5%	0.128	0.097	0.076	0.062	0.053	0.041
15%	0.127	0.096	0.076	0.062	0.052	0.041

Lastly, the tables for case 8 are given below:

Table 5.15. Displacement values at each period and strength ratio of Case 8.

Displacements (mm)						
SR/T	2	2.5	3	3.5	4	5
5%	192.83	238.42	273.85	306.03	340.38	409.00
7.5%	155.09	192.32	226.27	253.66	283.05	349.42
10%	124.78	157.73	188.96	222.18	256.35	317.60
12.5%	112.95	136.74	164.77	203.01	234.02	297.53
15%	105.39	126.66	148.79	188.00	233.02	287.35

Table 5.16. Base shear values at each period and strength ratio of Case 8.

Base Shear (V/W)						
SR/T	2	2.5	3	3.5	4	5
5%	0.210	0.157	0.123	0.100	0.084	0.063
7.5%	0.197	0.148	0.116	0.095	0.080	0.060
10%	0.185	0.140	0.111	0.092	0.078	0.059
12.5%	0.180	0.135	0.107	0.090	0.076	0.058
15%	0.177	0.132	0.105	0.088	0.076	0.058

Figure 5.8 shows the responses of the system under DD2, high hazard level and stiff soil condition (Case 7). Maximum base shear ratio is 0.138 (V/W). Displacement range is between 91 mm and 274 mm.

Figure 5.9 shows the responses of the system under DD2, high hazard level and soft soil condition (Case 8). For the smallest period and yield ratio, base shear is around 0.209 (V/W) and for the biggest period and yield ratio base shear is around 0.057 (V/W). Displacements differ from 105 mm to 409 mm. The effect of yield levels which are above 12.5% is not significant on ADRS chart when the period is 4 seconds. On

the other hand, for 2.5 and 3 seconds, differences in yield level dominate the responses of seismic isolation system.

There is not significant difference between minimum displacement responses of Case 7 and Case 8; it is approximately 1.5 cm.

As it is seen from Table 5.17; under the same soil conditions and hazard levels, DD2 design level imposes approximately half of the DD1 ADRS both maximum and minimum base shear values.

Table 5.17. Maximum and minimum responses of all cases.

DD1/DD2	DD1		DD2		DD1		DD2	
High/Moderate Hazard	HH		MH		HH		MH	
NEHRP C/D	C	D	C	D	C	D	C	D
Max.Displacement (mm)	595	755	494	647	274	409	237	341
Min.Displacement (mm)	226	217	166	176	91	105	92	95
Max. Base shear (V/M)	0.31	0.40	0.25	0.33	0.14	0.21	0.12	0.18
Min.Base shear (V/M)	0.08	0.11	0.07	0.09	0.04	0.06	0.03	0.05

In DD1 level, the maximum base shear reaches 0.4 (V/W) and in the worst case (Case 6) and maximum base shear never decreases under 0.12 (V/W) in any case.

When all graphs are considered the trend of the graphs is similar for the same soil type and design level but varying hazard level.

As expected, the values of base shear and displacement increase through high hazard level. When responses are observed, base shear ratio differs from 0.034 (W%) to 0.402 (W%). Among all cases displacement responses changes from 91 mm to 755 mm; approximately eight time difference in displacement may occur due to various seismic isolation and ground motion parameters.

In T=2.5-4.0 seconds range, the effect of increasing period decreases the increment ratio of base shear. Namely, the slope of horizontal lines reduces between these period ranges.

Results indicate that, periods between 2.5 s and 4 s are suitable for seismic isolation systems above and below of this period limits there are some inapplicable deformation and base shear values.

When yield level is above 12.5%, there is distortion in some cases hence; designers may need to make additional calculations to understand the real behavior of the seismic isolation system under existing conditions of the structure.

6. CONCLUSION

Nonlinear response history analyses are performed for different post-elastic periods and yield levels of seismic isolation systems and displacement and acceleration values are obtained. Ground motion sets composed of eleven pairs of earthquake recordings are scaled according to TBSDC (2018). Characteristic seismic isolation parameters are evaluated and inscribed in graphical form.

The ADRS methodology is practical tool for preliminary design of seismic isolation systems. The methodology enables to observe and evaluate demands and overall behavior of the system.

The ADRS charts can be used for all typical seismic isolation systems because the calculations are based on post-elastic periods and yield levels. The comparison of the different type of systems can be made in the same single chart and this feature makes it more feasible to evaluate all alternatives in decision process.

It is worth noting that, only for Case 2; at T=3 s periods, displacement responses are almost constant at yield level equal or higher than 10%. In further studies, analyses might be repeated using different ground motion data set to see if such an issue is raised by the excitation characteristics of the ground motion.

The ADRS graphs which make it possible to rapidly obtain the required parameters for preliminary design of seismic isolation systems quickly can be improved and standardized by making further analyses with vast ground motion data set.

REFERENCES

Bülbül Y.E., 2011, *Effect of Near-Field Ground Motions on Displacement Amplification Spectra in Inelastin Seismic Performance Evaluation*, Master of Science Thesis, Earthquake Engineering Department, KOERI, Boğaziçi University.

Chatzi E., 2017, *Lecture slides: Method of Finite Element Methods 2- Modeling of Hysteresis*, Institute of Structural Engineering, Department of Civil, Environment and Geomatic Engineering. Please See: https://www.ethz.ch/content/dam/ethz/special-interest/baug/ibk/structural-mechanics-dam/education/femII/BW_Model.pdf

Chatzidaki D., 2011, *Optimum design of base isolated RC structures*, Postgraduate Diploma Thesis, Interdisciplinary Postgraduate Program of Specialized Studies, Analysis and Design of Structures, Institute of Structural Analysis and Antiseismic Resarch, National Technical University of Athens.

Jones L., Aiken I., Black C., Whittaker D., Retamales R., Boroschek R., 2017, "An improved design methodology for seismic isolation systems using nonlinear response spectra", 16th *World Conferance on Earthquake Engineering*, 9-13 January, Santiago, Chile.

Jones L., Aiken I., Black C., Whittaker D., Şadan B., 2015a, "Nonlinear response spectra for isolation system design: case studies in Turkey, California and New Zealand", *3 TDMSK*, 14-16 October, Izmir, Turkey.

Jones L., Aiken I., Black C., Whittaker D., 2015b, "Design displacement and acceleration spectra for seismic isolation systems: New Zealand, San Francisco and Vancouver", 14th *World Conference on Seismic Isolation, Energy Dissipation and Active Vibration Control of Structures*, 9-11 September, San Diego, CA USA.

Jones L., Aiken I., Black C., Whittaker D., Ratemales R., Boroschek R., 2017, "An

Improved Design Methodology for Seismic Isolation Systems Using Nonlinear Response Spectra", 16th *World Conference on Earthquake Engineering*, 9-13 January, Santiago, Chile.

Naeim F., Kelly J. , 1999, *Design of Seismic Isolated Structures: From Theory to Practice*, John Wiley & Sons, Inc., Canada.

New Probabilistic Seismic Hazard Map of Turkey (TDTH), 2016, *Test Version*, Please See: http://www.afad.gov.tr/, 2017.

Pacific Earthquake Engineering Research (PEER) Center NGA-West 2 Ground Motion Database (NGA-West2), 2015, University of California, Berkeley, USA, Please See: https://ngawest2.berkeley.edu/, 2017.

PRISM for Earthquake Engineering Software 2.0.1 (PRISM), 2018, Earthquake Engineering Research Group, Departement of Architectural Engineering, INHA University, Incheon, South Korea. Please See: http://sem.inha.ac.kr/prism/, 2017.

Ryan K.L., Chopra A.K., 2004, "Estimation of Seismic Demands on Isolators Based on Nonlinear Analysis", *Journal of Structural Engineering, doi:10.1061/(ASCE)0733-9445(2004)130:3(392)*, ASCE, March, 2004

Turkish Building Seismic Design Code (TBSDC), 2018, *Draft Version.*

Tüzün C., Şadan B., 2017, *Technical Seminar: Introduction to design of seismically isolated structures*,IMO (Chamber of Civil Engineers), March, Bursa, Turkey.

Whittaker D., Jones L., 2013, "Design spectra for seismic isolation systems in Christchurch, New Zealand", *New Zealand Society for Earthquake Engineering Technical Conference*, 26-28 April, Wellington, New Zealand.

Whittaker D., Jones L., 2014, "Displacement and acceleration design spectra for seismic

isolation systems in Christchurch, New Zealand", *New Zealand Society for Earthquake Engineering Technical Conference*, 21-23 March, Auckland, New Zealand.